Pulsar Timing Arrays and NANOGrav 12.5 analysis

(a non expert view)

R. Ansari - Univ. Paris-Saclay & IJCLab

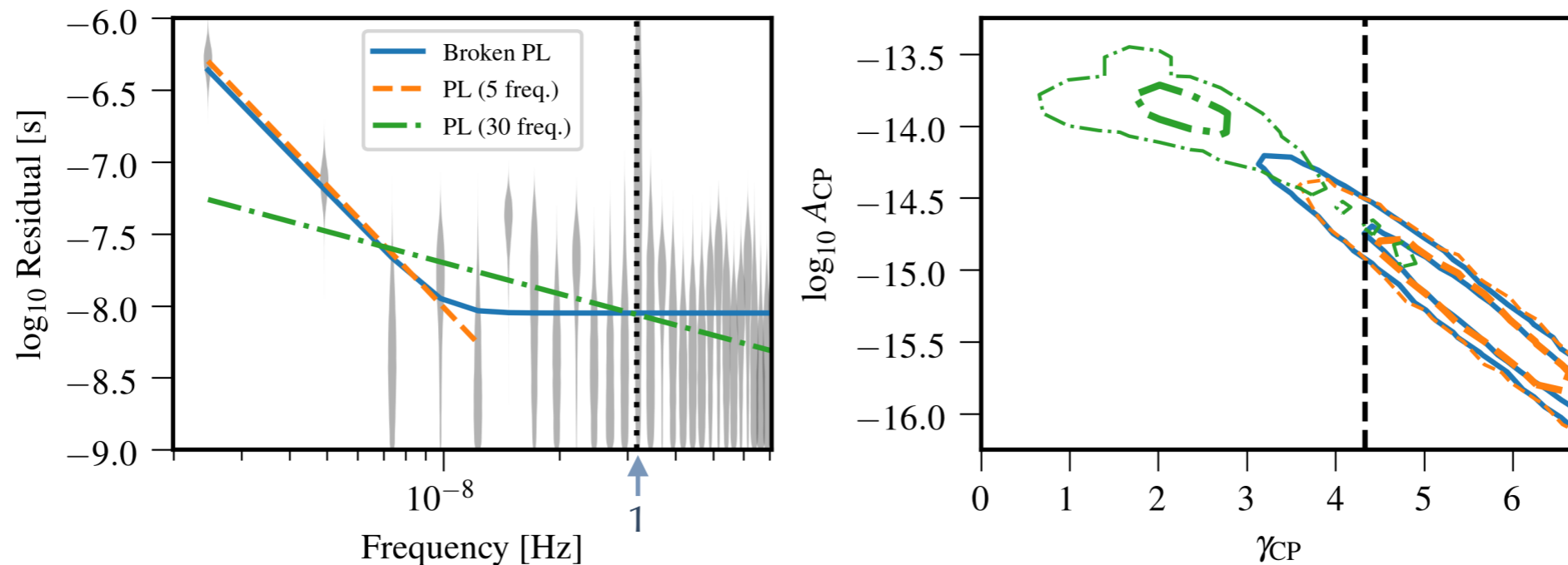# The NANOGrav 12.5-year Data Set:
Search For An Isotropic Stochastic Gravitational-Wave Background

Zaven Arzoumanian,[1] Paul T. Baker,[2] Harsha Blumer,[3,4] Bence Bécsy,[5] Adam Brazier,[6] Paul R. Brook,[3,4] Sarah Burke-Spolaor,[3,4,7] Shami Chatterjee,[6] Siyuan Chen,[8,9,10] James M. Cordes,[6] Neil J. Cornish,[5] Fronefield Crawford,[11] H. Thankful Cromartie,[12] Megan E. DeCesar,[13,14,*] Paul B. Demorest,[15] Timothy Dolch,[16] Justin A. Ellis,[17] Elizabeth C. Ferrara,[18] William Fiore,[3,4] Emmanuel Fonseca,[19] Nathan Garver-Daniels,[3,4] Peter A. Gentile,[3,4] Deborah C. Good,[20] Jeffrey S. Hazboun,[21,*] A. Miguel Holgado,[22] Kristina Islo,[23] Ross J. Jennings,[6] Megan L. Jones,[23] Andrew R. Kaiser,[3,4] David L. Kaplan,[23] Luke Zoltan Kelley,[24] Joey Shapiro Key,[21] Nima Laal,[25] Michael T. Lam,[26,27] T. Joseph W. Lazio,[28] Duncan R. Lorimer,[3,4] Jing Luo,[29] Ryan S. Lynch,[30] Dustin R. Madison,[3,4,*] Maura A. McLaughlin,[3,4] Chiara M. F. Mingarelli,[31,32] Cherry Ng,[33] David J. Nice,[13] Timothy T. Pennucci,[34,35,*] Nihan S. Pol,[3,4] Scott M. Ransom,[34] Paul S. Ray,[36] Brent J. Shapiro-Albert,[3,4] Xavier Siemens,[25,23] Joseph Simon,[28,37] Renée Spiewak,[38] Ingrid H. Stairs,[20] Daniel R. Stinebring,[39] Kevin Stovall,[15] Jerry P. Sun,[25] Joseph K. Swiggum,[13,*] Stephen R. Taylor,[40] Jacob E. Turner,[3,4] Michele Vallisneri,[28] Sarah J. Vigeland,[23] Caitlin A. Witt[3,4]

The NANOGrav Collaboration

Figure 1. Posteriors for a common-spectrum process in NG12, as recovered with four models: free-spectrum (gray violin plots in left panel), broken power law (solid blue lines and contours), five frequency power law (dashed orange lines and contours), and 30 frequency power law (dot-dashed green lines and contours). In the left panel, the violin plots show marginalized posteriors of

Search v0.5.6 released 2020-02-24   Feedback?

nanograv   Title ▾   Search

◉ Show abstracts   ○ Hide abstracts

Advanced Search

50 ▾ results per page.   Sort results by   Announcement date (newest first) ▾   Go

1. arXiv:2009.14663 [pdf, other] astro-ph.CO   gr-qc   hep-th

   Is the NANOGrav signal a hint of dS decay during inflation?

   Authors: Hao-Hao Li, Gen Ye, Yun-Song Piao

   Abstract: As suggested by the swampland conjectures, de Sitter (dS) space might be highly unstable if it exists at all. During inflation, the short-lived dS states will decay through a cascade of the first-order phase transition (PT). We find that the gravitational waves (GWs) yielded by such a PT will be "reddened" by subsequent dS expansion, which may result in a slightly red-tilt stochastic GWs backgroun... ▽ More

   Submitted 30 September, 2020; originally announced September 2020.

   Comments: 9 pages,2 figures

2. arXiv:2009.14174 [pdf, other] astro-ph.CO   astro-ph.HE

   NANOGrav signal from MHD turbulence at QCD phase transition in the early universe

   Authors: A. Neronov, A. Roper Pol, C. Caprini, D. Semikoz

   Abstract: NANOGrav collaboration has recently reported evidence for existence of stochastic gravitationalwave background in the 1-100 nHz frequency range. We argue that such background could have been produced by magneto-hydrodynamic (MHD) turbulence at the first-order cosmological QCD phase transition. NANOGrav measurements suggest the magnetic field parameters: the comovingfield strength close to microGau... ▽ More

   Submitted 29 September, 2020; originally announced September 2020.

   Comments: 5 pages, 2 figures

3. arXiv:2009.13893 [pdf, other] astro-ph.CO   hep-ph

   NanoGrav 12.5-yr data and different stochastic Gravitational wave background sources

   Authors: Ligong Bian, Jing Liu, Ruiyu Zhou

   Abstract: The NANOGrav Collaboration recently observed a strong evidence for a stochastic common-spectrum process in the pulsar timing data. In this work, we evaluate the possibility to interpret this process as stochastic gravitational wave backgrounds produced from first-order phase transitions, cosmic strings, domain walls, and large amplitude curvature perturbations.

   Submitted 29 September, 2020; originally announced September 2020.

   Comments: 18 pages, 5 figures, 1 table; comments welcome

4. arXiv:2009.13452 [pdf, other] hep-ph   astro-ph.CO   astro-ph.GA   gr-qc

   Gravitational wave complementarity and impact of NANOGrav data on gravitational leptogenesis: cosmic strings

   Authors: Rome Samanta, Satyabrata Datta

   Abstract: In seesaw mechanism, if right handed (RH) neutrino masses are generated dynamically by a gauged $U(1)$ symmetry breaking, a stochastic gravitational wave background (SGWB) sourced by a cosmic string network could be a potential probe of leptogenesis. We show that the leptogenesis mechanism that facilitates the dominant production of lepton asymmetry via quantum effects of right-handed neutrino... ▽ More

   Submitted 30 September, 2020; v1 submitted 28 September, 2020; originally announced September 2020.

   Comments: 16 pages, 4 figures, typo corrected, refs. updated

8. **From NANOGrav to LIGO with metastable cosmic strings**

   Authors: Wilfried Buchmuller, Valerie Domcke, Kai Schmitz

   Abstract: We interpret the recent NANOGrav results in terms of a stochastic gravitational wave background from metastable cosmic strings. The observed amplitude of a stochastic signal can be translated into a range for the cosmic string tension and the mass of magnetic monopoles arising in theories of grand unification. In a sizable part of the parameter space, this interpretation predicts a large stochasti... ▽ More

   Submitted 22 September, 2020; originally announced September 2020.

   Comments: 5 pages, 2 figures

   Report number: CERN-TH-2020-157, DESY 20-154

9. arXiv:2009.10327 [pdf, other] hep-ph   gr-qc

   NANOGrav results and Dark First Order Phase Transitions

   Authors: Andrea Addazi, Yi-Fu Cai, Qingyu Gan, Antonino Marciano, Kaiqiang Zeng

   Abstract: The recent NANOGrav evidence of a common-source stochastic background provides a hint to Gravitational Waves (GW) radiation from the Early Universe. We show that this result can be interpreted as a GW spectrum produced from First Order Phase Transitions (FOPTs) around a temperature in the KeV-MeV window. Such a class of FOPTs at temperatures much below the electroweak scale can be naturally envisa... ▽ More

   Submitted 23 September, 2020; v1 submitted 22 September, 2020; originally announced September 2020.

   Comments: More details and results on possible WDM-inspired GW spectra added, including more recent numerical tools in the subject. New references added. The main conclusions are substantially unchanged

10. arXiv:2009.09754 [pdf, other] astro-ph.CO   gr-qc   hep-ph

   Gravitational Waves and Dark Radiation from Dark Phase Transition: Connecting NANOGrav Pulsar Timing Data and Hubble Tension

   Authors: Yuichiro Nakai, Motoo Suzuki, Fuminobu Takahashi, Masaki Yamada

   Abstract: Recent pulsar timing data reported by the NANOGrav collaboration may indicate the existence of a stochastic gravitational wave background around $f \sim 10^{-8}$ Hz. We explore a possibility to generate such low-frequency gravitational waves from a dark sector phase transition. Assuming that the dark sector is completely decoupled from the visible sector except via the gravitational interaction, w... ▽ More

   Submitted 27 September, 2020; v1 submitted 21 September, 2020; originally announced September 2020.

   Comments: 9 pages, 4 figures; v2: suppression factor for the sound-wave period included, figures updated, conclusions unchanged

   Report number: TU-1109; IPMU20-0100

11. arXiv:2009.08268 [pdf, other] astro-ph.CO   gr-qc   hep-ph

   NANOGrav Hints to Primordial Black Holes as Dark Matter

   Authors: V. De Luca, G. Franciolini, A. Riotto

   Abstract: The NANOGrav Collaboration has recently published a strong evidence for a stochastic common-spectrum process that may be interpreted as a stochastic gravitational wave background. We show that such a signal can be explained by second-order gravitational waves produced during the formation of primordial black holes from the collapse of sizeable scalar perturbations generated during inflation. This... ▽ More

   Submitted 17 September, 2020; originally announced September 2020.

   Comments: 5 pages, 1 figure

12. arXiv:2009.07832 [pdf, other] astro-ph.CO

   Did NANOGrav see a signal from primordial black hole formation?

   Authors: Ville Vaskonen, Hardi Veermäe

   Abstract: We show that the recent NANOGrav result can be interpreted as a stochastic gravitational wave signal associated to formation of primordial black holes from high-amplitude curvature perturbations. The indicated amplitude and power of the gravitational wave spectrum agrees well with formation of primordial seeds for supermassive black holes.

   Submitted 30 September, 2020; v1 submitted 16 September, 2020; originally announced September 2020.

   Comments: 7 pages, 4 figures

The NANOGrav 12.5-year Data Set:
Search For An Isotropic Stochastic Gravitational-Wave Background

Zaven Arzoumanian,[1] Paul T. Baker,[2] Harsha Blumer,[3,4] Bence Bécsy,[5] Adam Brazier,[6] Paul R. Brook,[3,4] Sarah Burke-Spolaor,[3,4,7] Shami Chatterjee,[6] Siyuan Chen,[8,9,10] James M. Cordes,[6] Neil J. Cornish,[5] Fronefield Crawford,[11] H. Thankful Cromartie,[12] Megan E. DeCesar,[13,14,*] Paul B. Demorest,[15] Timothy Dolch,[16] Justin A. Ellis,[17] Elizabeth C. Ferrara,[18] William Fiore,[3,4] Emmanuel Fonseca,[19] Nathan Garver-Daniels,[3,4] Peter A. Gentile,[3,4] Deborah C. Good,[20] Jeffrey S. Hazboun,[21,*] A. Miguel Holgado,[22] Kristina Islo,[23] Ross J. Jennings,[6] Megan L. Jones,[23] Andrew R. Kaiser,[3,4] David L. Kaplan,[23] Luke Zoltan Kelley,[24] Joey Shapiro Key,[21] Nima Laal,[25] Michael T. Lam,[26,27] T. Joseph W. Lazio,[28] Duncan R. Lorimer,[3,4] Jing Luo,[29] Ryan S. Lynch,[30] Dustin R. Madison,[3,4,*] Maura A. McLaughlin,[3,4] Chiara M. F. Mingarelli,[31,32] Cherry Ng,[33] David J. Nice,[13] Timothy T. Pennucci,[34,35,*] Nihan S. Pol,[3,4] Scott M. Ransom,[34] Paul S. Ray,[36] Brent J. Shapiro-Albert,[3,4] Xavier Siemens,[25,23] Joseph Simon,[28,37] Renée Spiewak,[38] Ingrid H. Stairs,[20] Daniel R. Stinebring,[39] Kevin Stovall,[15] Jerry P. Sun,[25] Joseph K. Swiggum,[13,*] Stephen R. Taylor,[40] Jacob E. Turner,[3,4] Michele Vallisneri,[28] Sarah J. Vigeland,[23] Caitlin A. Witt[3,4]

The NANOGrav Collaboration

9 Sep 2020

ABSTRACT

We search for an isotropic stochastic gravitational-wave background (GWB) in the 12.5-year pulsar timing data set collected by the North American Nanohertz Observatory for Gravitational Waves (NANOGrav). Our analysis finds strong evidence of a stochastic process, modeled as a power-law, with common amplitude and spectral slope across pulsars. The Bayesian posterior of the amplitude for a $f^{-2/3}$ power-law spectrum, expressed as characteristic GW strain, has median 1.92×10^{-15} and 5%–95% quantiles of 1.37–2.67×10^{-15} at a reference frequency of $f_{\mathrm{yr}} = 1 \ \mathrm{yr}^{-1}$. The Bayes factor in favor of the common-spectrum process versus independent red-noise processes in each pulsar exceeds 10,000. However, we find no statistically significant evidence that this process has quadrupolar spatial correlations, which we would consider necessary to claim a GWB detection consistent with General Relativity. We find that the process has neither monopolar nor dipolar correlations, which may arise from, for example, reference clock or solar-system ephemeris systematics, respectively. The amplitude posterior has significant support above previously reported upper limits; we explain this in terms of the Bayesian priors assumed for intrinsic pulsar red noise. We examine potential implications for the supermassive black hole binary population under the hypothesis that the signal is indeed astrophysical in nature.

https://arxiv.org/abs/2009.04496

✤ Nanohertz Gravitational waves , stochastic GWB

   ✤ Pulsar Timing Arrays & interferometric GW detection

https://arxiv.org/abs/1811.08826

✤ From radio signals to a possible GWB detection

   ✤ Pulsar signals

   ✤ Timing models

   ✤ Residual analysis

https://arxiv.org/abs/2005.06490 (NG12)

https://arxiv.org/abs/2005.06495

https://arxiv.org/abs/1801.02617 (NG11gwb)

https://arxiv.org/abs/1201.6641

https://arxiv.org/abs/1509.02165 (EPTA)

https://www.nature.com/articles/217709a0

NanoHz GW

based on *Astrophysics of NanoHz GW ,*
A&A review , 2019

REVIEW ARTICLE

Check for
updates
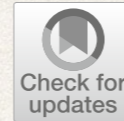
The astrophysics of nanohertz gravitational waves

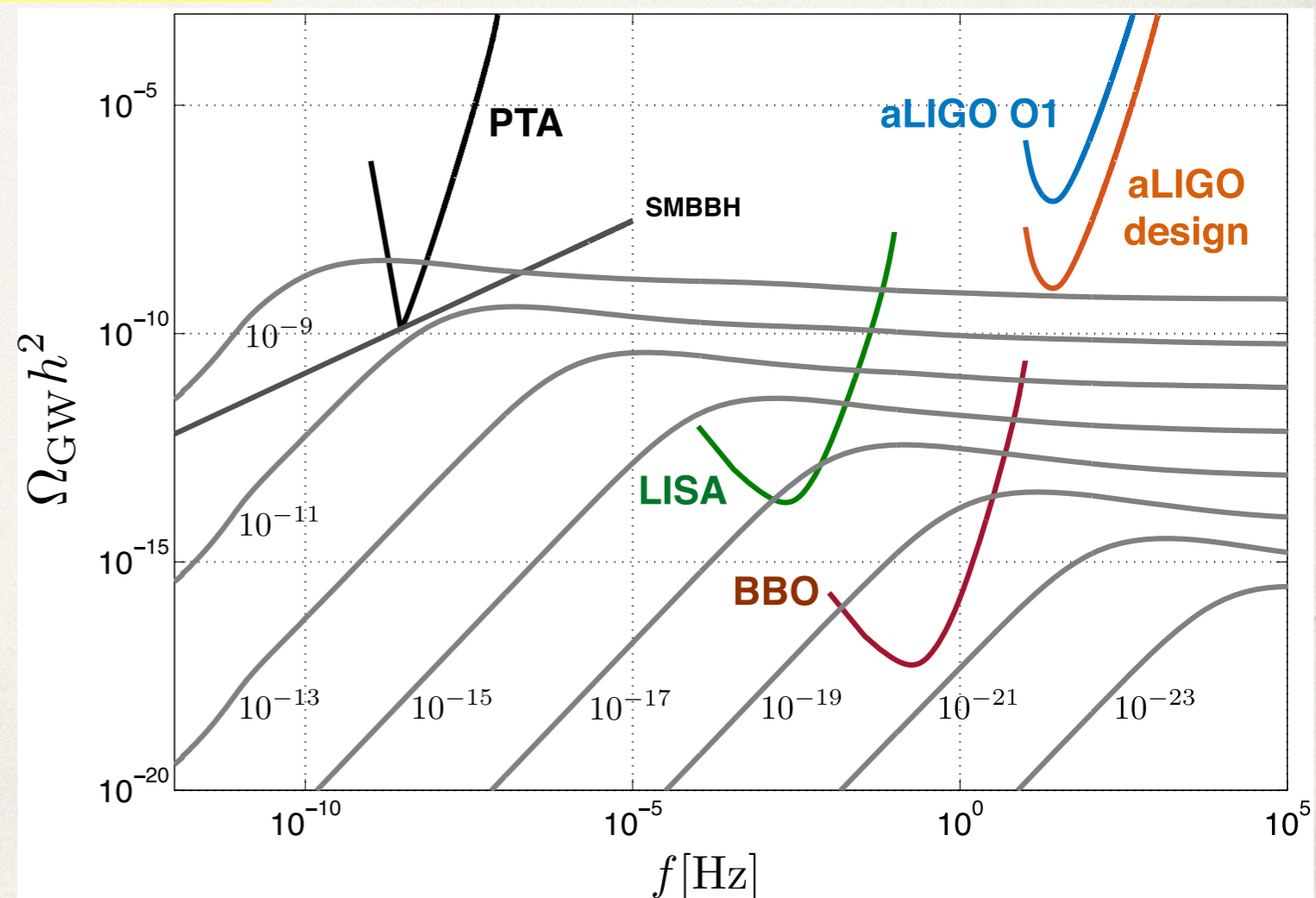Sarah Burke-Spolaor, et al. *[full author details at the end of the article]*

https://arxiv.org/abs/1811.08826

Abstract

Pulsar timing array (PTA) collaborations in North America, Australia, and Europe, have been exploiting the exquisite timing precision of millisecond pulsars over decades of observations to search for correlated timing deviations induced by gravitational waves (GWs). PTAs are sensitive to the frequency band ranging just below 1 nanohertz to a few tens of microhertz. The discovery space of this band is potentially rich with

Fig. 10 Plot of the gravitational wave spectrum in terms of the dimensionless parameter Ω, as a function of frequency in hertz. The figure shows cosmic (super)string spectra for $p = 1$ for values of the (dimensionless) string tension $G\mu/c^2$ in the range of 10^{-23}–10^{-9}, as well as the spectrum produced by supermassive binary black holes (SMBBH), along with the current and future experimental constraints. The figure is from Blanco-Pillado et al. (2018)
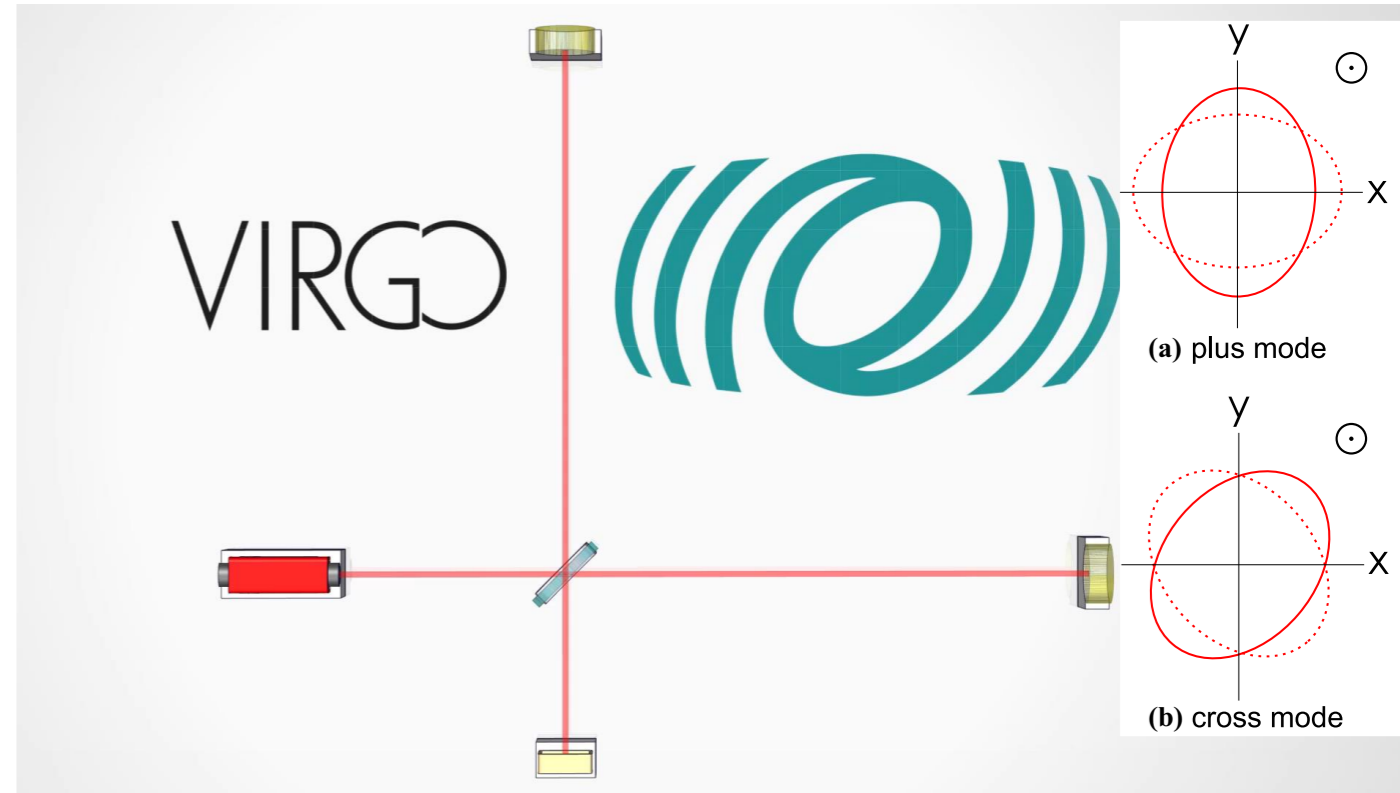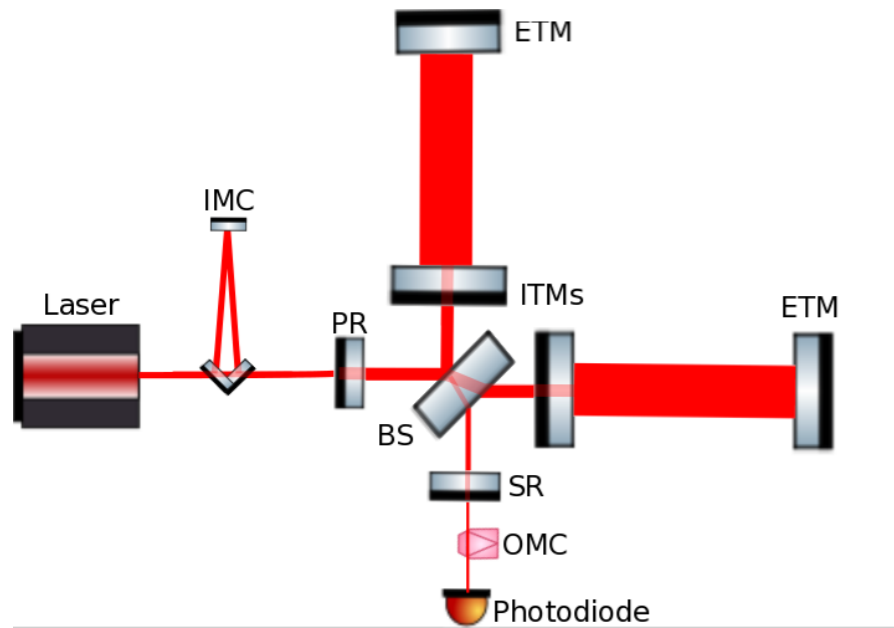
Dual recycled Fabry-Perot interferometer

LIGO and Virgo will use dual recycled Fabry-Perot interferometers including input mode cleaner and output mode cleaner

https://indico.cern.ch/event/806261/

Detecting gravitational waves with an interferometer

During our detection of GW150914 the mirrors moved by about 10^{-18} m

(a) plus mode

(b) cross mode

Virgo sensitivity: best value about 50 Mpc

Significant improvement with respect to the best sensitivity obtained in O2. However, we see a flat noise contribution at mid-frequencies, significant noise around 50 Hz. Virgo uses 18 W of power

Last Sensitivity (Mon Sep 2 21:04:32 2019 UTC)

- Virgo sensitivity (at GPS=1251493490) 48 Mpc
- O2 Reference Sensitivity (GPS=1189375218) BNS range=30 Mpc
- O3 Observing Scenario (60-85 Mpc)
- elog43891 sensitivity (36 Mpc)

Start=Sep 2 21:04:32 2019 duration=300 sec   Freq (Hz)
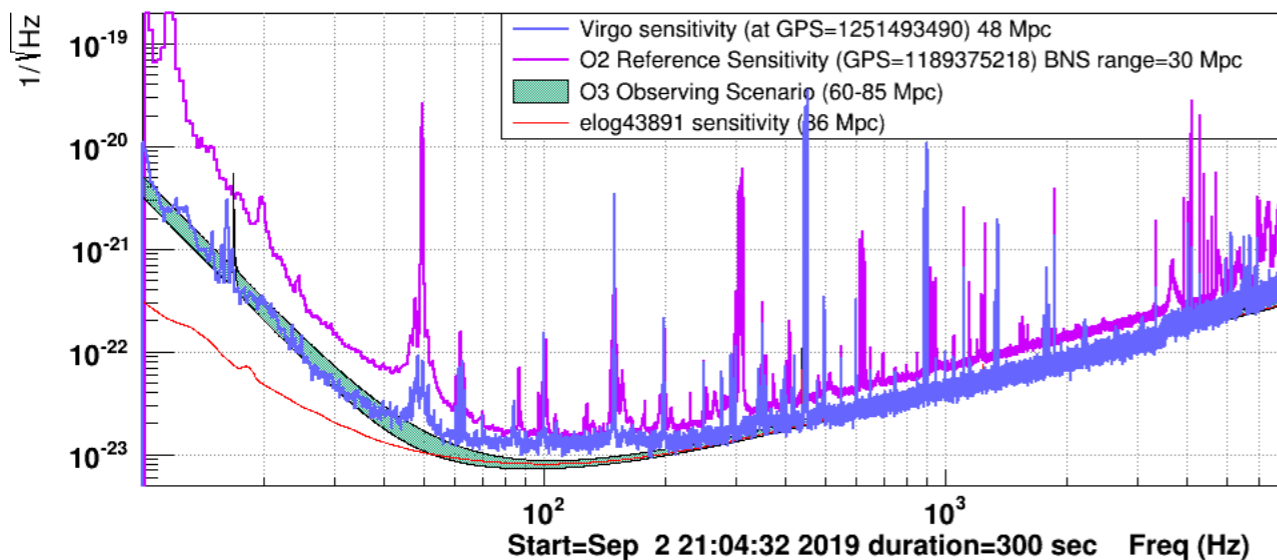
VIRGO/LIGO : path length difference detection , a small fraction of wavelength (λ_{opt}~ 1 μm), optical path length ~ 1000 km (multiple reflection in the FP cavities) → 100 Hz , and $10^{-6} \lambda_{opt}$ for h ~10^{-18}

Nanohertz GW with PTA

- Pulsars : (super ?) stable clocks , located in the galaxies, at kpc typical distances

- GW frequencies $\nu \sim 10^{-8} \text{Hz} \longrightarrow \lambda_{GW} \sim 3.\, 10^{16}\, \text{m} \sim 1\text{pc}$

- A nanoHz GW strength $h \sim 10^{-15}$ would then produce a path difference of ~ 30 meters, or a time delay of ~ 30 ns

- GW wave detection would be based on observing few tens of ns change in the pulsar period, over few years duration (1 year $\sim 3.\, 10^7\text{s}$)

- the changes should be correlated between pulsars, when the delay is caused by the earth term

2 Pulsar timing in brief

Here, we introduce the critical concepts for understanding how PTAs can access their target science.

Timing residuals: Evidence of GWs can be seen by the influence they have on the arrival time of pulsar signals at the Earth. The measured versus predicted arrival time of pulses, as a function of time, is referred to as the timing residuals.

Pulsar versus Earth term: A propagating GW will pass both the pulsar and Earth, affecting their local space–time at different times. Pulsar timing can detect a GW's passage through an individual pulsar ("pulsar term"), and can detect a wave's passage through the Earth ("Earth term") as a signal correlated between pulsars.

Correlation analysis: While we can detect the Earth or pulsar term in one pulsar, a GW can only be confidently detected by observing the correlated influence of the GW on multiple pulsars, demonstrating a dominantly quadrupolar signature.

GW signals:

- *Continuous waves* from orbiting binary black holes.
- *GW bursts* from single-encounter supermassive black hole (SMBH) pairs and cosmic strings.
- *Bursts with memory*, singular, rapid and permanent step changes in space time that can accompany SMBH binary (SMBHB) coalescence and cosmic strings.
- *GW background*, the combined sum from all sources of GW emission.

SMBH :
Super Massive Black Hole

SMBBH :
Super Massive Binary Black Holes

https://arxiv.org/abs/1811.08826
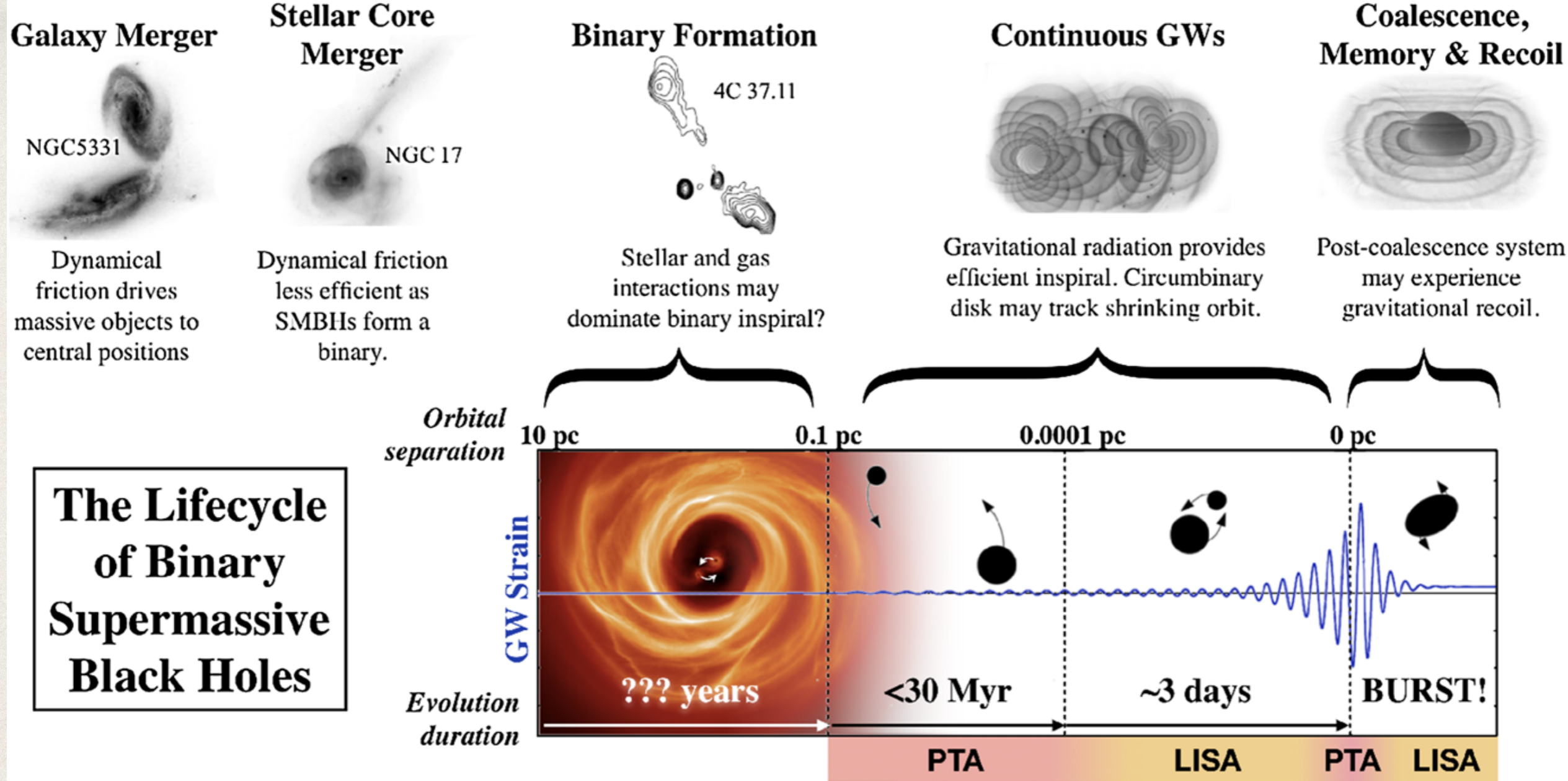
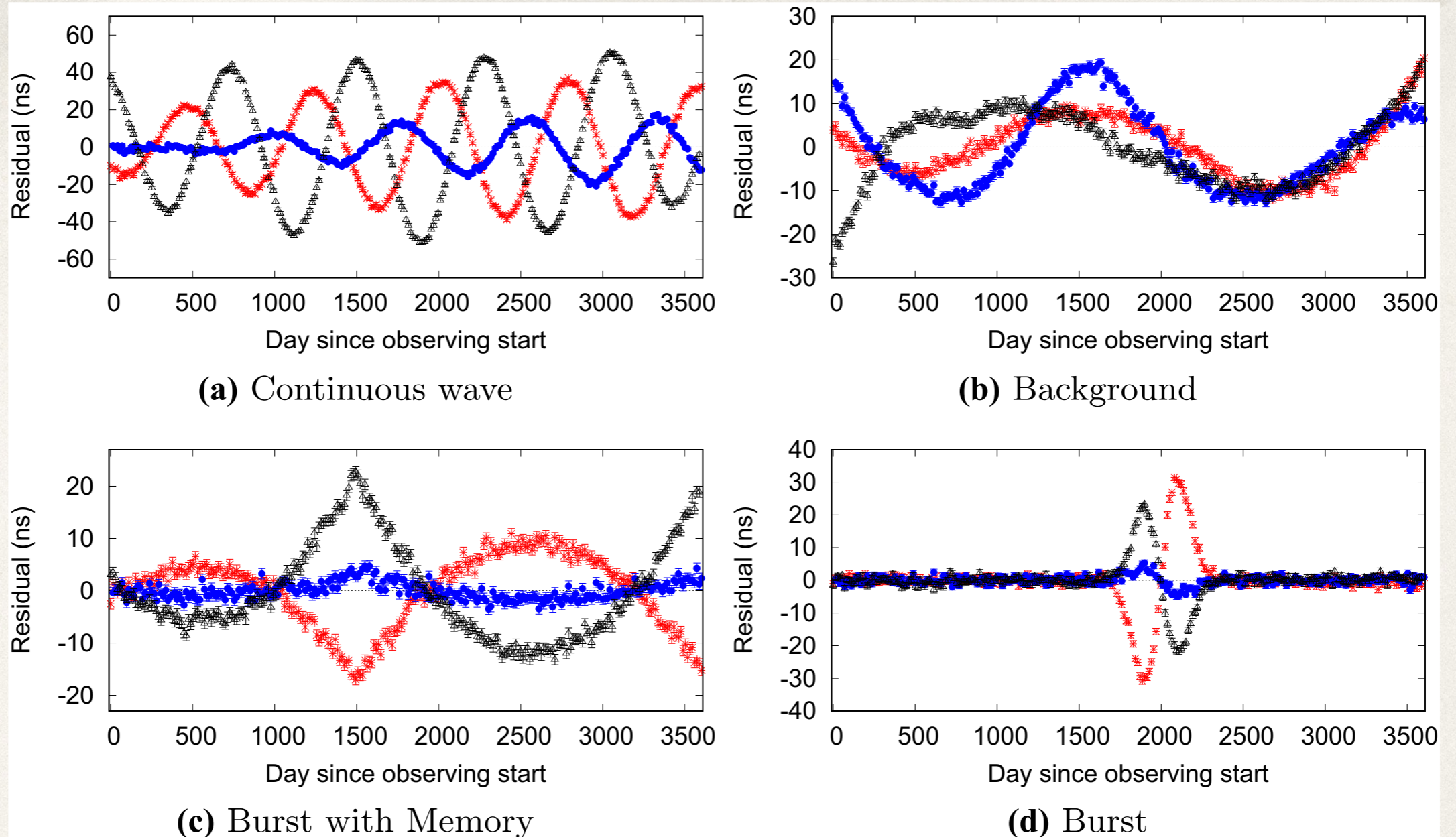**Fig. 3** Binary SMBHs can form during a major merger. Pulsar timing arrays' main targets are continuous-wave binaries within ∼0.1 pc separation (second panel in the lower figure; Sect. 3.1.2), although we may on rare occasion detect "GW memory" from a binary's coalescence (Favata 2010, Sect. 3.1.3). Millions of such binaries will contribute to a stochastic GW background, also detectable by PTAs (Sect. 3.1.4). A major unknown in both binary evolution theory and GW prediction is the means by which a binary progresses from ∼10 pc separations down to ∼0.1 pc, after which the binary can coalesce efficiently due to GWs (e. g., Begelman et al. 1980). If it cannot reach sub-parsec separations, a binary may "stall" indefinitely; such occurrences en masse can cause a drastic reduction in the ensemble GWs from this population. Alternately, if the binary interacts excessively with the environment within 0.1 pc orbital separations, the expected strength and spectrum of the expected GWs will change. Image credits: Galaxies, Hubble/STSci; 4C37.11, Rodriguez et al. (2006); Simulation visuals, C. Henze/NASA; Circumbinary accretion disk, C. Cuadra

https://arxiv.org/abs/1811.08826

(a) Continuous wave **(b)** Background **(c)** Burst with Memory **(d)** Burst
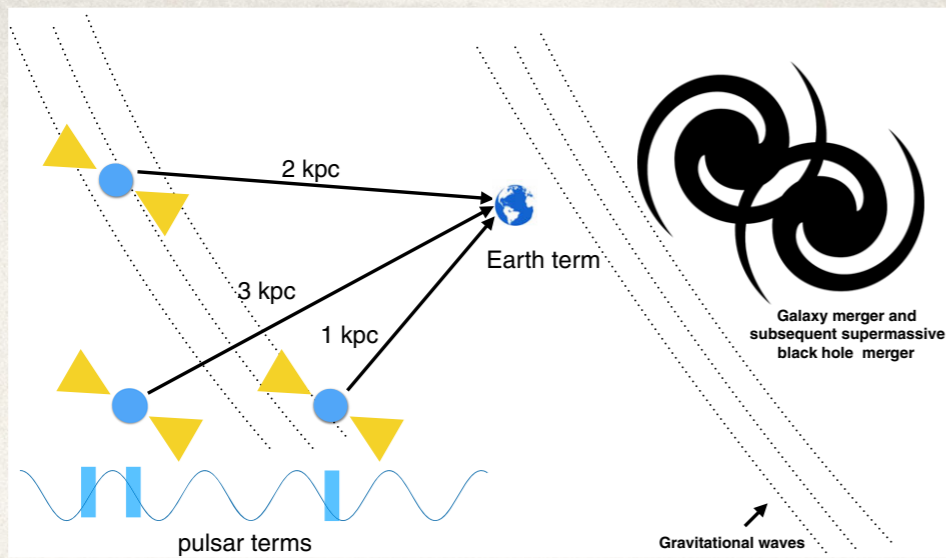
Scale: ± 20-50 ns

Fig. 1 Each panel shows pulsar timing residuals for three pulsars (black triangles, red stars, blue circles) simulated with weekly observing cadence and 1 ns of white noise in their arrival times. The pulsar-to-pulsar variations demonstrate how the quadrupolar signature of GWs will manifest as correlated timing residuals in distinct pulsars. Note that 1 ns is not a noise level yet achieved for any pulsar; however, here it allows us to demonstrate each observable signal type with a high signal-to-noise ratio. Panels are: **a** continuous waves from an equal mass 10^9 $M_\odot$ SMBHB at redshift $z = 0.01$. The distortion from a perfect sinusoid is caused by self-interference from the pulsar term (Sect. 2.2). In this case, the pulsar term has a lower frequency because we see the effects on the pulsar from an earlier phase in the SMBHB's inspiral evolution. This interferes with the Earth term, which takes a direct path from the source to Earth and therefore is a view of a more advanced stage of evolution. **b** A GW background with $h_c = 10^{-15}$ and $\alpha = -2/3$. **c** A memory event of $h = 5 \times 10^{-15}$, whose wavefront passes the Earth on day 1500. **d** A burst source with an arbitrary waveform

https://arxiv.org/abs/1811.08826

10^9 M$_\odot$ SMBHB at z=0.01 !
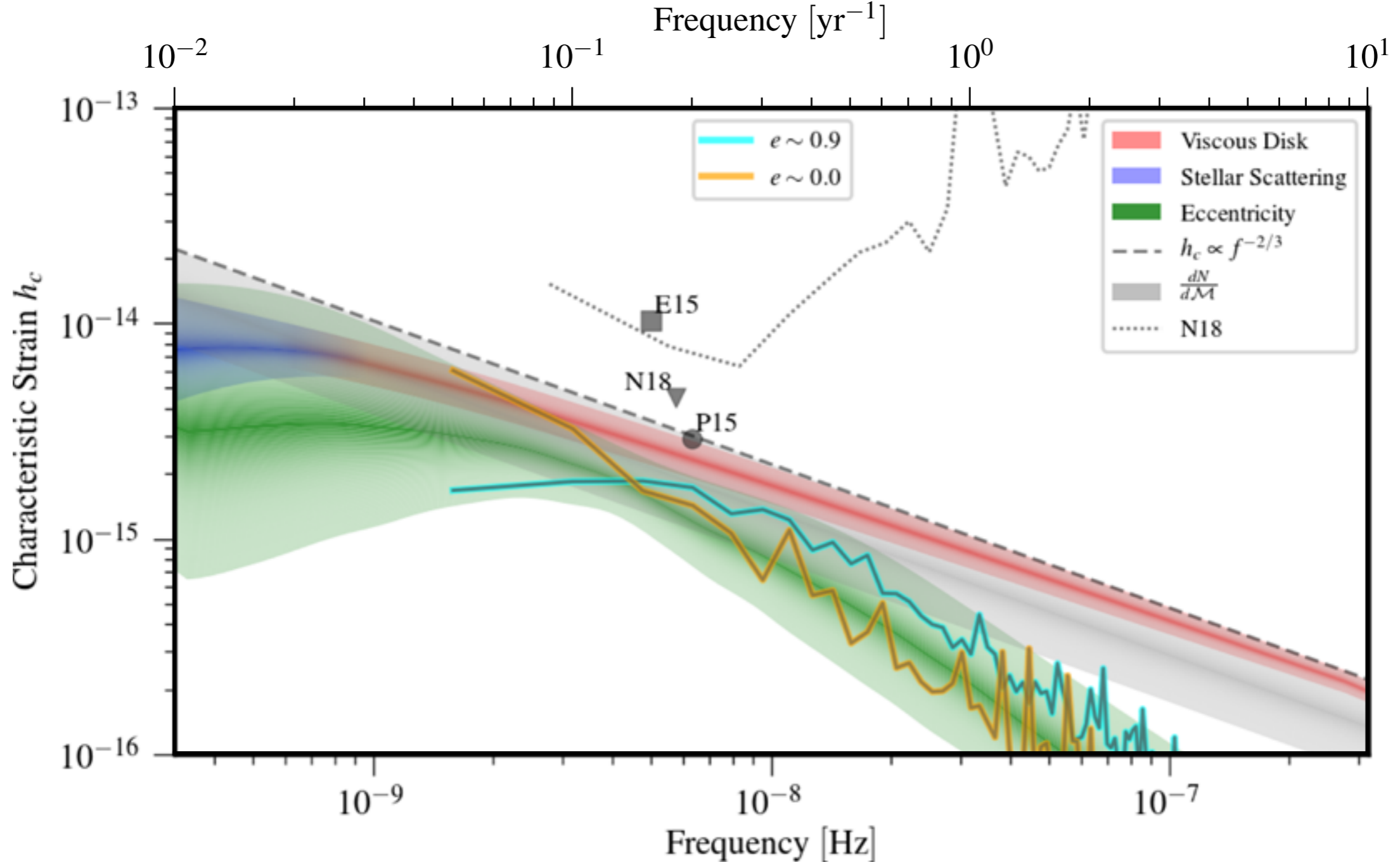
Fig. 4 The GW spectrum at nanohertz frequencies from supermassive black hole binaries. We adapted the data from the SMBH binary populations and evolutionary models of Kelley et al. (2017a) and Kelley et al. (2017b), highlighting the effects of variations in particular binary model parameters on the resulting GW spectrum. The dashed black line is the spectrum using only the population mass distribution and assuming GW-driven evolution, and the gray-shaded region represents the uncertainty in the overall distribution of SMBHB in the universe. The cyan (orange) line is the GW background from a particular realization of an SMBHB population using a high (low) eccentricity model. The time sampling corresponds to a PTA with duration of 20 years and a cadence of 0.05 year. The NANOGrav 11 year detection sensitivity and GW background upper limits (Arzoumanian et al. 2018a) are illustrated with a gray dotted line and triangle, respectively, while the EPTA (Lentati et al. 2015) and PPTA (Shannon et al. 2015) upper limits are denoted by a square and circle, respectively. We note that the PPTA limit appears to be most constraining; however, it is known to be sensitive to the choice of planetary ephemeris; this effect has been accounted for in subsequent analysis of other PTA data and results in less constraining limits (Arzoumanian et al. 2018a). *Note:* the shaded regions are schematic

Expected stochastic GW background spectrum from SMBBH and Nanograv (2018) & EPTA limits (2015)
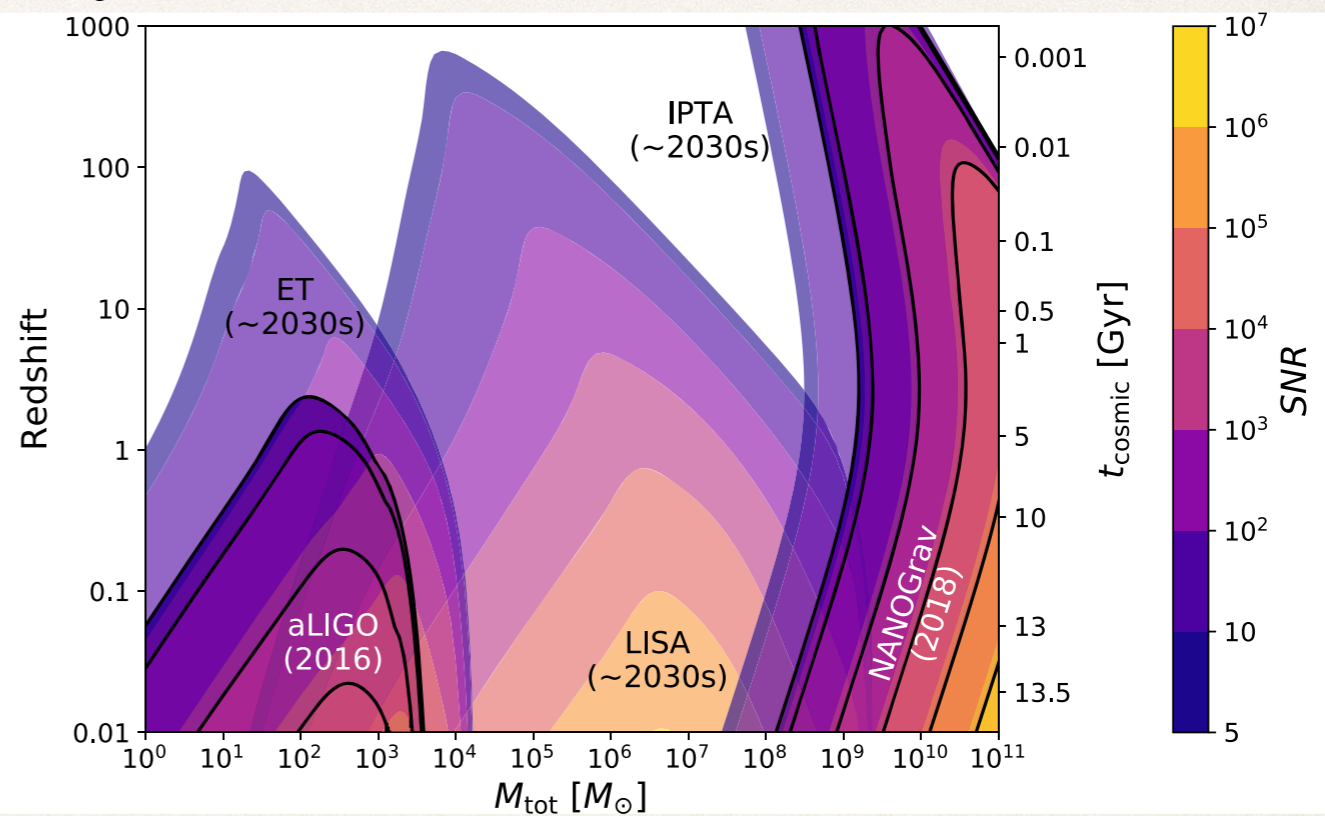
Fig. 6 Gravitational waves spanning thousands of years in a binary's evolutionary cycle can be detected from a continuous GW source by using the pulsar term. As an example, we have drawn a few pulsars with line-of-sight path length differences to the Earth. These relative time delays between the pulsar terms can be used to probe the evolution and the dynamics of an SMBHB systems over these many thousands of years. Right: a major galaxy merger leads to the creation of an SMBHB, emitting nanohertz GWs. Left: the pulsar term from each pulsar probes a different part of the SMBHB evolution, since they are all at different distances from the Earth. The blue sinusoid is a cartoon of the GW waveform and shows that the pulsar terms can be coherently concatenated to probe the binary's evolution, allowing one to measure, e.g., the spin of the SMBHB (Mingarelli et al. 2012)

← Illustration of the Pulsar term in probing GW using PTA

https://arxiv.org/abs/1811.08826

Probing black hole masses with GW using different technics [Interferometer Ground, Space , PTA] →

Fig. 16 LIGO, LISA, and PTAs have complementary coverage to study the full range of black hole masses at various stages of the Universe. Here we show the approximate signal-to-noise ratio for the complementary wavebands of these three instruments as they are currently (darker shading/black contours) and in the early- to mid-2030's era (lighter shading). This plot focuses only on *individual* (rather than stochastic) black hole detections. All curves assume instrument-limited sensitivity, without an astrophysical background. Individual inspiral/coalescence events at high redshift will be detectable by LISA, while

North American Nanohertz Observatory for Gravitational Waves
A National Science Foundation Physics Frontiers Center

NANOGrav
Physics Frontiers Center

Research
Astro2020
Data
Events
Telescopes
Outreach

About the NANOGrav PFC

Pulsar timing arrays are on track to detect long-period gravitational waves by measuring their effects on the light-travel times of pulses from rotating neutron stars (pulsars). NANOGrav monitors a set of pulsars

News

Damage to the Arecibo Telescope

The damage to the NSF's Arecibo telescope from the falling support cable earlier this month will result in significant disruption to telescope operations, dealing a blow to radio astronomy, planetary science, and aeronomy. Arecibo has been the most sensitive radio telescope in the world for most of the last half

Arecibo & GBT radio telescopes

http://nanograv.org

The European Pulsar Timing Array

EPTA

Home | Gravitational Waves | Pulsars | Telescopes | People | LEAP | References | Outreach | AOM

Welcome to the EPTA website

The European Pulsar Timing Array is a multinational European collaboration of pulsar astronomers. Our aim is to increase the precision and quality of pulsar science results by combining the efforts and resources of the various member insititutions and telescopes.
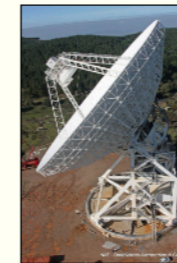
http://www.epta.eu.org

The Effelsberg Radio Telescope
Effelsberg, Germany

The Lovell Telescope
Cheshire, United Kingdom

The Nançay Decimetric Radio Telescope
Nançay, France

The Sardinia Radio Telescope
Pranu Sanguni, Italy

The Westerbork Synthesis Radio Telescope
Westerbork, The Netherlands

http://www.ipta4gw.org

PPTA

Parkes Pulsar Timing Array
Welcome!

The Parkes Pulsar Timing Array (PPTA) project is a combined effort from astronomers an very first detection of gravitational waves in the pulsar timing band.

The PPTA project was formed in 2004 as a collaboration between CSIRO Astronomy and members from across the globe. The PPTA is now a member of the International Pulsar

The 64 metre Parkes Radio Telescope located in Parkes, New South Wales, Australia, is an array of fast-spinning stars in our Milky Way Galaxy emitting beams of radio waves,

https://www.atnf.csiro.au/research/pulsar/ppta/

Caption: CSIRO's Parkes radio telescope. Credit: David McClenaghan, CSIRO

INTERNATIONAL PULSAR TIMING ARRAY
IPTA

European Pulsar Timing Array limits on continuous gravitational waves from individual supermassive black hole binaries

S. Babak,[1]★ A. Petiteau,[2]★ A. Sesana,[1,3]★ P. Brem,[1] P. A. Rosado,[4,5] S. R. Taylor,[6,7]
A. Lassus,[8,9] J. W. T. Hessels,[10,11] C. G. Bassa,[10,12] M. Burgay,[13] R. N. Caballero,[8]
D. J. Champion,[8] I. Cognard,[9,14] G. Desvignes,[8] J. R. Gair,[7] L. Guillemot,[9,14]
G. H. Janssen,[10,12] R. Karuppusamy,[8] M. Kramer,[8,12] P. Lazarus,[8] K. J. Lee,[15]
L. Lentati,[16] K. Liu,[8] C. M. F. Mingarelli,[3,8,17] S. Osłowski,[8,18] D. Perrodin,[13]
A. Possenti,[13] M. B. Purver,[12] S. Sanidas,[11,12] R. Smits,[10] B. Stappers,[12]
G. Theureau,[9,14,19] C. Tiburzi,[13,20] R. van Haasteren,[17] A. Vecchio[3]
and J. P. W. Verbiest[8,18]

noise only. Depending on the adopted detection algorithm, the 95 per cent upper limit on the sky-averaged strain amplitude lies in the range $6 \times 10^{-15} < A < 1.5 \times 10^{-14}$ at $5\,\mathrm{nHz} < f < 7\,\mathrm{nHz}$. This limit varies by a factor of five, depending on the assumed source position and the most constraining limit is achieved towards the positions of the most sensitive pulsars in the timing array. The most robust upper limit – obtained via a full Bayesian analysis searching simultaneously over the signal and pulsar noise on the subset of ours six best pulsars – is $A \approx 10^{-14}$. These limits, the most stringent to date at $f < 10\,\mathrm{nHz}$, exclude the presence of sub-centiparsec binaries with chirp mass $\mathcal{M}_c > 10^9\,\mathrm{M}_\odot$ out to a distance of about 25 Mpc, and with $\mathcal{M}_c > 10^{10}\,\mathrm{M}_\odot$ out to a distance of about 1 Gpc ($z \approx 0.2$). We show that state-of-the-art SMBHB population models predict <1 per cent probability of detecting a CGW with the current EPTA data set, consistent with the reported non-detection. We stress, however, that PTA limits on individual CGW have improved by almost an order of magnitude in the last five

https://arxiv.org/abs/1509.02165

The data …

Claimed signal based on the 12 years Narrow Band analysis of the data

https://arxiv.org/abs/2005.06490 (NG12)

Wide band 12 years analysis

https://arxiv.org/abs/2005.06495

NanoGrav 5 years (2013) - 17 pulsars analysis

https://arxiv.org/abs/1201.6641

ABSTRACT

We present time-of-arrival measurements and timing models of 47 millisecond pulsars (MSPs) observed from 2004 to 2017 at the Arecibo Observatory and the Green Bank Telescope by the North American Nanohertz Observatory for Gravitational Waves (NANOGrav). The observing cadence was three to four weeks for most pulsars over most of this time span, with weekly observations of six sources. These data were collected for use in low-frequency gravitational wave searches and for other astrophysical purposes. We detail our observational methods and present a set of time-of-arrival (TOA) measurements, based on "narrowband" analysis, in which many TOAs are calculated within narrow radio-frequency bands for data collected simultaneously across a wide bandwidth. A separate set of "wideband" TOAs will be presented in a companion paper. We detail a number of methodological changes compared to our previous work which yield a cleaner and more uniformly processed data set. Our timing models include several new astrometric and binary pulsar measurements, including previously unpublished values for the parallaxes of PSRs J1832−0836 and J2322+2057, the secular derivatives of the projected semi-major orbital axes of PSRs J0613−0200 and J2229+2643, and the first detection of the Shapiro delay in PSR J2145−0750. We report detectable levels of red noise in the time series for fourteen pulsars. As a check on timing model reliability, we investigate the stability of astrometric parameters across data sets of different lengths. We report flux density measurements for all pulsars observed. Searches for stochastic and continuous gravitational waves using these data will be subjects of forthcoming publications.

Narrow band 12.5 years analysis

NG12

ABSTRACT

We present a new analysis of the profile data from the 47 millisecond pulsars comprising the 12.5-year data set of the North American Nanohertz Observatory for Gravitational Waves (NANOGrav), which is presented in a parallel paper (Alam et al. *submitted to ApJS*; NG12.5). Our reprocessing is performed using "wideband" timing methods, which use frequency-dependent template profiles, simultaneous time-of-arrival (TOA) and dispersion measure (DM) measurements from broadband observations, and novel analysis techniques. In particular, the wideband DM measurements are used to constrain the DM portion of the timing model. We compare the ensemble timing results to NG12.5 by examining the timing residuals, timing models, and noise model components. There is a remarkable level of agreement across all metrics considered. Our best-timed pulsars produce encouragingly similar results to those from NG12.5. In certain cases, such as high-DM pulsars with profile broadening, or sources that are weak and scintillating, wideband timing techniques prove to be beneficial, leading to more precise timing model parameters by $10 - 15\%$. The high-precision multi-band measurements in several pulsars indicate frequency-dependent DMs. The TOA volume is reduced by a factor of 33, which may ultimately facilitate computational speed-ups for complex pulsar timing array analyses. This first wideband pulsar timing data set is a stepping stone, and its consistent results with NG12.5 assure us that such data sets are appropriate for gravitational wave analyses.

Wide band 12.5 years analysis

LIMITS ON THE STOCHASTIC GRAVITATIONAL WAVE BACKGROUND FROM THE NORTH AMERICAN NANOHERTZ OBSERVATORY FOR GRAVITATIONAL WAVES

P. B. Demorest[1], R. D. Ferdman[2], M. E. Gonzalez[3], D. Nice[4], S. Ransom[1], I. H. Stairs[3], Z. Arzoumanian[5,6], A. Brazier[7],
S. Burke-Spolaor[8], S. J. Chamberlin[9], J. M. Cordes[7], J. Ellis[9], L. S. Finn[10], P. Freire[11], S. Giampanis[9], F. Jenet[12],
V. M. Kaspi[2], J. Lazio[8], A. N. Lommen[13], M. McLaughlin[14], N. Palliyaguru[14], D. Perrodin[13], R. M. Shannon[15],
X. Siemens[9], D. Stinebring[16], J. Swiggum[14], and W. W. Zhu[3]

Table 1
List of Observed Millisecond Pulsars: Basic Parameters and Observing Setups

Source	P (ms)	dP/dt (10^{-20})	DM (pc cm^{-3})	P_b (d)	Average Flux Density (mJy)[a] (327 MHz)	(430 MHz)	(820 MHz)	(1.4 GHz)	(2.3 GHz)	Obs
J0030+0451	4.87	1.02	4.33	⋯	⋯	19.9	⋯	1.4	⋯	AO
J0613−0200	3.06	0.96	38.78	1.2	⋯	⋯	5.3	2.0	⋯	GBT
J1012+5307	5.26	1.71	9.02	0.6	⋯	⋯	7.6	3.9	⋯	GBT
J1455−3330	7.99	2.43	13.57	76.2	⋯	⋯	2.0	1.1	⋯	GBT
J1600−3053	3.60	0.95	52.33	14.3	⋯	⋯	3.1	2.3	⋯	GBT
J1640+2224	3.16	0.28	18.43	175.5	⋯	10.9	⋯	1.0	⋯	AO
J1643−1224	4.62	1.85	62.42	147.0	⋯	⋯	12.3	4.2	⋯	GBT
J1713+0747	4.57	0.85	15.99	67.8	⋯	⋯	8.8	6.3	3.6	AO,GBT
J1744−1134	4.07	0.89	3.14	⋯	⋯	⋯	7.6	2.6	⋯	GBT
J1853+1308	4.09	0.87	30.57	115.7	⋯	⋯	⋯	0.2	⋯	AO
B1855+09	5.36	1.78	13.30	12.3	⋯	24.6	⋯	4.0	⋯	AO
J1909−3744	2.95	1.40	10.39	1.5	⋯	⋯	3.4	1.4	⋯	GBT
J1910+1256	4.98	0.97	34.48	58.5	⋯	⋯	⋯	0.2	⋯	AO
J1918−0642	7.65	2.57	26.60	10.9	⋯	⋯	4.5	1.8	⋯	GBT
B1953+29	6.13	2.97	104.50	117.3	⋯	⋯	⋯	1.0	0.1	AO
J2145−0750	16.05	2.98	9.03	6.8	⋯	⋯	12.3	3.2	⋯	GBT
J2317+1439	3.45	0.24	21.90	2.5	32.2	9.9	⋯	⋯	⋯	AO

Table 2
Overview and Results from Timing Model Fits

Source	No. of TOAs[a]	No. of Parameters DM	Profile	Other[b]	rms (μs)	Fit χ^2	Epoch-averaged rms / median σ_t (μs)[c] Low-band[d]	High-band	Combined	Figure Nos.
J0030+0451	545	20	26	7	0.604	1.44	0.019/0.38	0.328/0.35	0.148/0.37	4
J0613−0200	1113	34	45	12	0.781	1.21	0.021/0.17	0.519/0.50	0.178/0.30	5
J1012+5307	1678	52	53	14	1.327	1.40	0.192/0.69	0.345/0.65	0.276/0.67	6
J1455−3330	1100	37	53	12	4.010	1.01	0.363/1.66	1.080/2.97	0.787/2.35	7
J1600−3053	625	21	31	14	1.293	1.45	0.233/0.52	0.141/0.27	0.163/0.34	8
J1640+2224	631	23	26	12	0.562	4.36	0.057/0.20	0.601/0.52	0.409/0.22	9
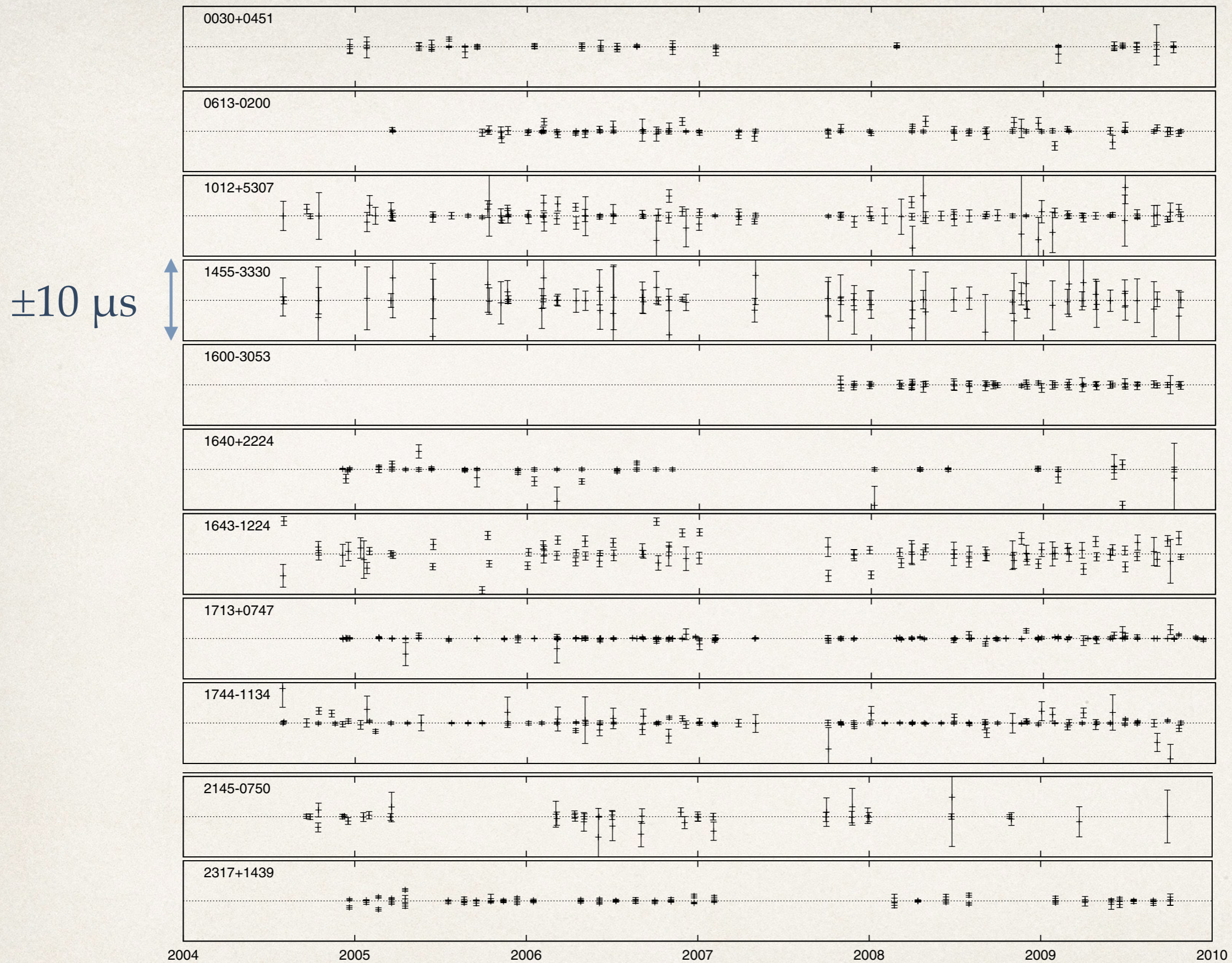
Figure 1. Overview of timing residuals for all sources, showing observational cadence and coverage during the five-year time span. The gap in 2007 was due to an extended maintenance period at both telescopes. The full scale of the y-axis is $10\,\mu$s in all cases.

https://arxiv.org/abs/1201.6641

The NANOGrav 12.5-year Data Set: Wideband Timing of 47 Millisecond Pulsars

Md F. Alam,[1] Zaven Arzoumanian,[2] Paul T. Baker,[3] Harsha Blumer,[4,5] Keith E. Bohler,[6] Adam Brazier,[7]
Paul R. Brook,[4,5] Sarah Burke-Spolaor,[4,5] Keeisi Caballero,[6] Richard S. Camuccio,[6] Rachel L. Chamberlain,[1]

ABSTRACT

https://arxiv.org/abs/2005.06495

We present a new analysis of the profile data from the 47 millisecond pulsars comprising the 12.5-year data set of the North American Nanohertz Observatory for Gravitational Waves (NANOGrav), which is presented in a parallel paper (Alam et al. *submitted to ApJS*; NG12.5). Our reprocessing is performed using "wideband" timing methods, which use frequency-dependent template profiles, simultaneous time-of-arrival (TOA) and dispersion measure (DM) measurements from broadband observations, and novel analysis techniques. In particular, the wideband DM measurements are used to constrain the DM portion of the timing model. We compare the ensemble timing results to NG12.5 by examining

All data were collected either at the 305-m Arecibo Observatory (AO), or the 100-m Robert C. Byrd Green Bank Telescope (GBT). Any pulsar that is visible with the more sensitive AO dish is observed there, otherwise we observe it with the GBT. Arecibo was used to observe 27 sources, while 24 sources have data from the GBT. We regularly observe J1713+0747 and B1937+21 (a.k.a. J1939+2134) with both facilities.

Most pulsars are observed once every 3–4 weeks, with six sources being observed weekly:

All pulsars are observed with receivers in two widely separated frequency bands during each epoch in order to measure propagation effects from the ISM, including variations in the DM. At Arecibo, these frequency bands are two of three possible receivers centered around 430 MHz (~70 cm), 1.4 GHz (~20 cm, "L-band"), and 2.1 GHz (~15 cm, "S-band"); the use of the 327 MHz (~90 cm) receiver for one source, J2317+1439, has been discontinued since the end of 2013. At the GBT, all sources are observed with the 820 MHz (~35 cm) and L-band (1.4 GHz) receivers. The receiver turret at Arecibo
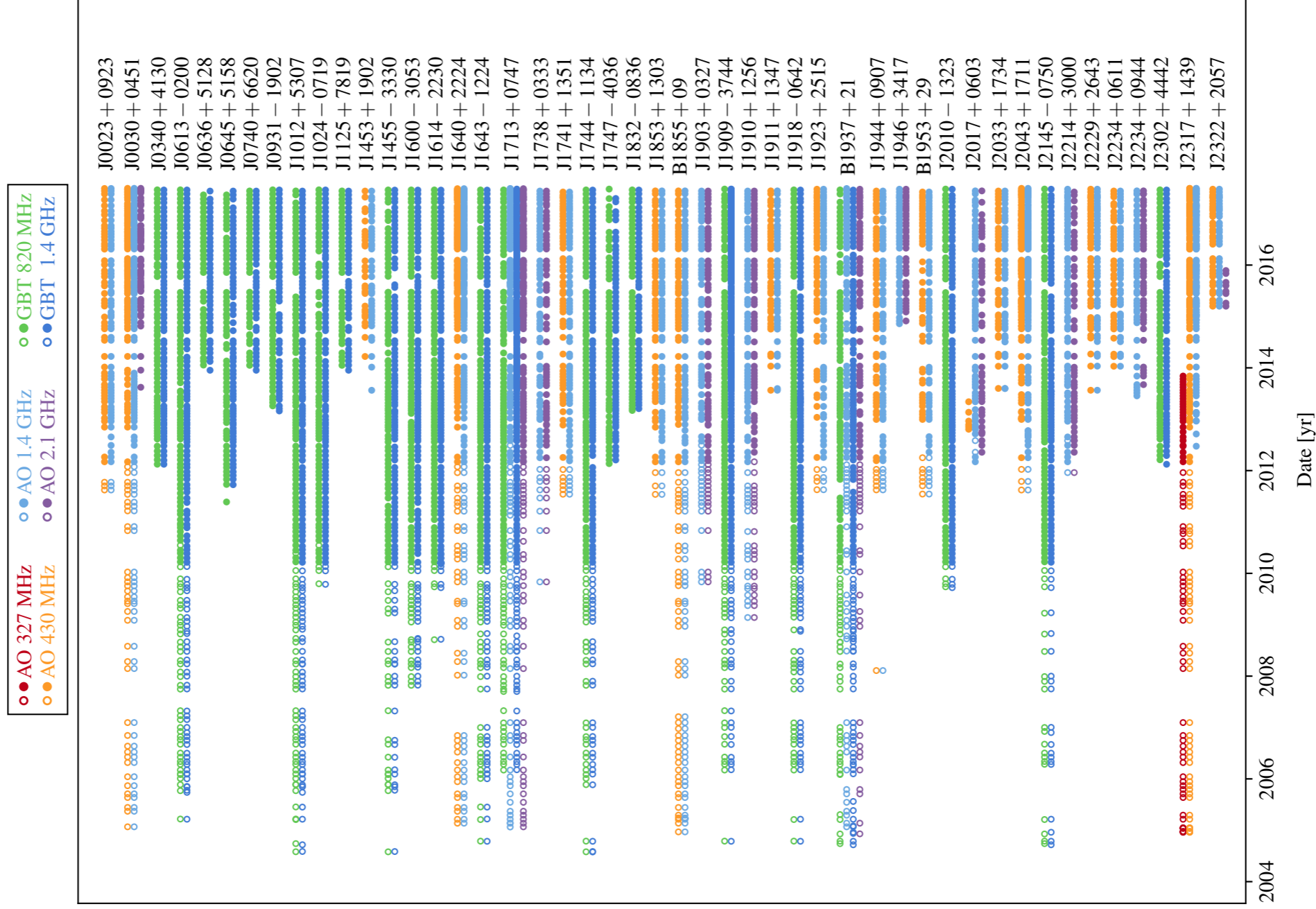
Between approximately 2010 and 2012 we transitioned from the 64 MHz bandwidth capable ASP and GASP data acquisition backend instruments at Arecibo and the GBT, respectively (Demorest 2007a), to the 800 MHz bandwidth capable PUPPI and GUPPI instruments (Ford et al. 2010; DuPlain et al. 2008). Details of these

The ASP and GASP data are left at their native 4 MHz frequency channel resolution, whereas the PUPPI and GUPPI data are frequency-averaged to have channel bandwidths in the range 1.5–12.5 MHz, depending on the frequency range observed.

| | Backends | | | | | | | |
| Telescope Receiver | ASP/GASP | | | | PUPPI/GUPPI | | | |
	Data Span[b]	Frequency Range[c] [MHz]	Usable Bandwidth[d] [MHz]	ΔDM Delay[e] [μs]	Data Span[b]	Frequency Range[c] [MHz]	Usable Bandwidth[d] [MHz]	ΔDM Delay[e] [μs]
Arecibo								
327	$2005.0 - 2012.0$	$315 - 339$	34	2.86	$2012.2 - 2017.5$	$302 - 352$	50	6.00
430	$2005.0 - 2012.3$	$422 - 442$	20	1.03	$2012.2 - 2017.5$	$421 - 445$	24	1.23
L-wide	$2004.9 - 2012.3$	$1380 - 1444$	64	0.09	$2012.2 - 2017.5$	$1147 - 1765$	603	0.91
S-wide	$2004.9 - 2012.6$	$2316 - 2380$	64	0.02	$2012.2 - 2017.5$	$1700 - 2404^{f}$	460	0.36
GBT								
Rcvr_800	$2004.6 - 2011.0$	$822 - 866$	64	0.30	$2010.2 - 2017.5$	$722 - 919$	186	1.52
Rcvr1_2	$2004.6 - 2010.8$	$1386 - 1434$	48	0.07	$2010.2 - 2017.5$	$1151 - 1885$	642	0.98

The NANOGrav 12.5-year Wideband Data Set

Parallax / proper motion
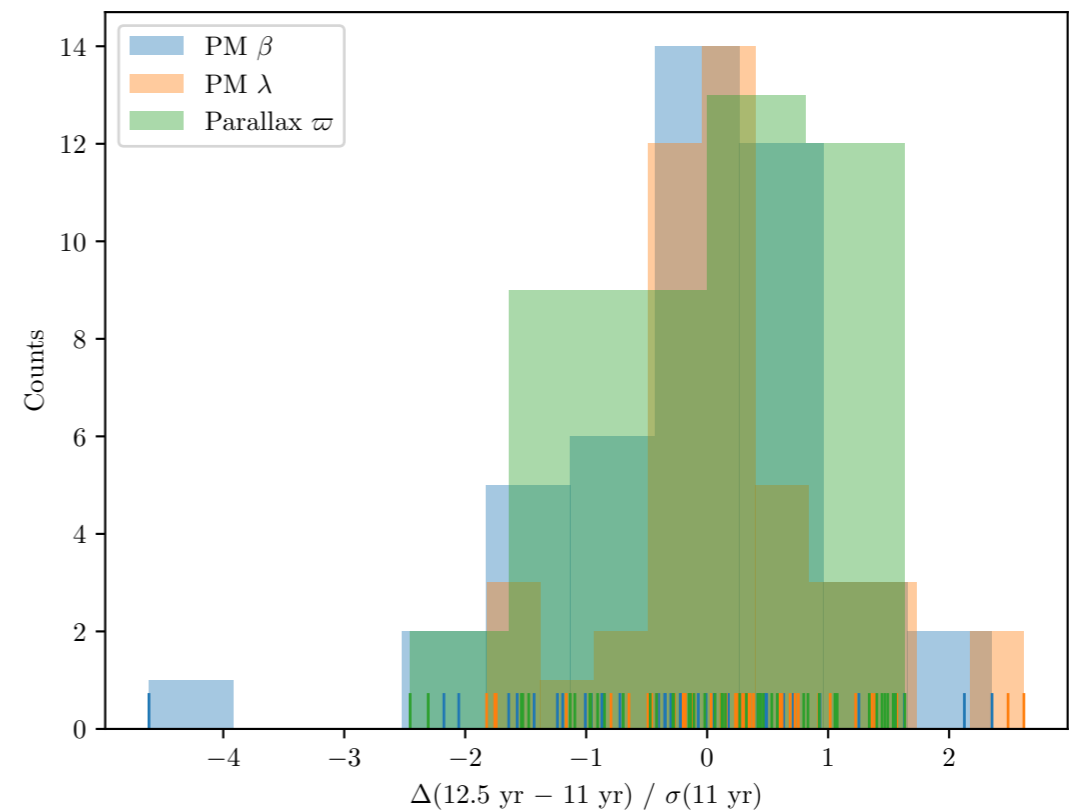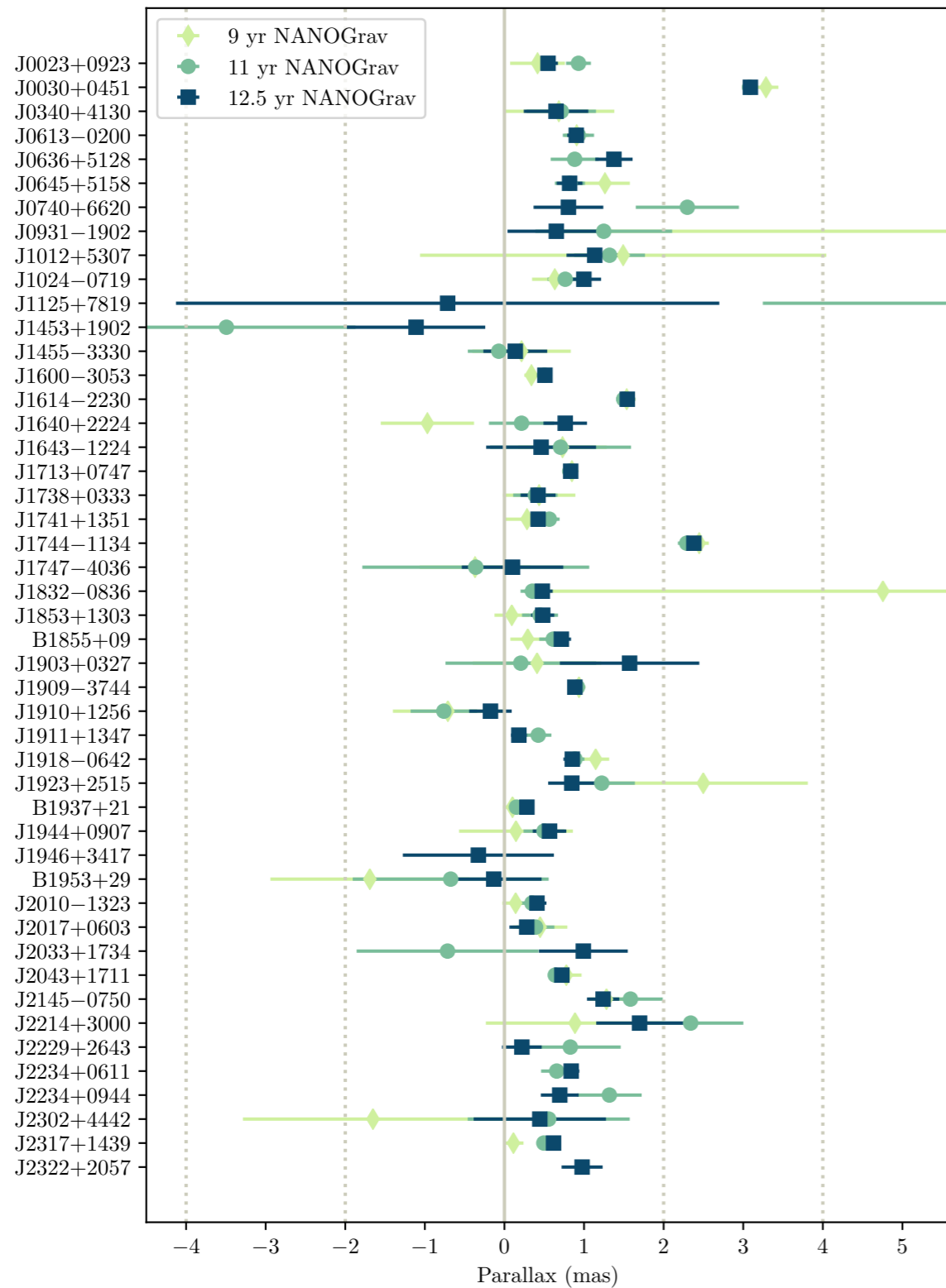
Figure 4. Comparison of astrometric measurements across NG11 and the current 12.5-year data set. The differe... proper motion (μ_β, μ_λ) and parallax ϖ are shown in units of the uncertainty in the 11-year measurement (σ_{11}). Th... shows binned histograms of each type of measurement, with all individual measurements superimposed as short verti... at the bottom of the figure. The value of μ_β for PSR J2214+3000 is an outlier at $-4.6\,\sigma$; the rest are reasonably consi... discussed in the text.

https://arxiv.org/abs/2005.06490

Timing model

- ❖ Radio pulses need to be reconstructed (instrumental calibration) and their arrival times (TOA) compared to a timing model to derive residuals

- ❖ Major ingredients of the timing model :

  - ❖ Accurate solar system ephemeris

  - ❖ intrinsic pulsar parameters : spin, spin down-rate

  - ❖ Astrometry: position (two angles), proper motion, parallax

  - ❖ For binary pulsars, Keplerian orbital parameters (period, eccentricity, semi major / minor axis …)

  - ❖ Dispersion measure, and possibly an intrinsic pulsar red-noise …

Table 2. Basic Pulsar Parameters and TOA Statistics

Source	P (ms)	dP/dt (10^{-20})	DM (pc cm^{-3})	P_b (d)	327 MHz	430 MHz		820 MHz		1.4 GHz		2.1 GHz		Span (yr)
						Median scaled TOA uncertainty^a (μs) / Number of epochs							
J0023+0923	3.05	1.14	14.3	0.1	$\cdots$	0.063	62	$\cdots$		0.556	68	$\cdots$		6.0
J0030+0451	4.87	1.02	4.3	-	$\cdots$	0.214	175	$\cdots$		0.424	187	1.558	71	12.4
J0340+4130	3.30	0.70	49.6	-	$\cdots$	$\cdots$		0.868	68	2.108	71	$\cdots$		5.3
J0613−0200	3.06	0.96	38.8	1.2	$\cdots$	$\cdots$		0.109	134	0.582	135	$\cdots$		12.2
J0636+5128	2.87	0.34	11.1	0.1	$\cdots$	$\cdots$		0.279	39	0.579	42	$\cdots$		3.5

Table 3. Summary of Timing Model Fits

Source	Number of TOAs	S	A	B	DM	FD	J	Full	White	$A_{\rm red}$	$\gamma_{\rm red}$	$\log_{10} B$	Figure Number
		\multicolumn{6}{c}{Number of Fit Parameters^a}			\multicolumn{2}{c}{RMS^b (μs)}		\multicolumn{3}{c}{Red Noise^c}		
J0023+0923	12516	3	5	9	67	4	1	0.285	$\cdots$	$\cdots$	$\cdots$	1.21	6
J0030+0451	12543	3	5	0	190	4	2	25.157	0.200	0.003	−6.3	>2	7
J0340+4130	8069	3	5	0	74	4	1	0.446	$\cdots$	$\cdots$	$\cdots$	−0.21	8
J0613−0200	13201	3	5	8	139	2	1	0.486	0.178	0.123	−2.1	>2	9
J0636+5128	21374	3	5	6	44	1	1	0.640	$\cdots$	$\cdots$	$\cdots$	−0.09	10
J0645+5158	7893	3	5	0	79	2	1	0.207	$\cdots$	$\cdots$	$\cdots$	−0.20	11
J0740+6620	3328	3	5	7	44	1	1	0.132	$\cdots$	$\cdots$	$\cdots$	−0.17	12
J0931−1902	3712	3	5	0	57	0	1	0.452	$\cdots$	$\cdots$	$\cdots$	−0.15	13

Few rows of tables in https://arxiv.org/abs/2005.06490

Back track 50 years …

1974 Nobel Prize in Physics : Sir Martin Ryle & Antony Hewish

Observation of a Rapidly Pulsating Radio Source

by

A. HEWISH
S. J. BELL
J. D. H. PILKINGTON
P. F. SCOTT
R. A. COLLINS

Mullard Radio Astronomy Observatory,
Cavendish Laboratory,
University of Cambridge

Unusual signals from pulsating radio sources have been recorded at the Mullard Radio Astronomy Observatory. The radiation seems to come from local objects within the galaxy, and may be associated with oscillations of white dwarf or neutron stars.

In July 1967, a large radio telescope operating at a frequency of 81·5 MHz was brought into use at the Mullard Radio Astronomy Observatory. This instrument was designed to investigate the angular structure of compact radio sources by observing the scintillation caused by the irregular structure of the interplanetary medium[1]. The initial survey includes the whole sky in the declination range $-08° < \delta < 44°$ and this area is scanned once a week. A large fraction of the sky is thus under regular surveillance. Soon after the instrument was brought into operation it was noticed that signals which appeared at first to be weak sporadic interference were repeatedly observed at a fixed declination and right ascension; this result showed that the source could not be terrestrial in origin.

Systematic investigations were started in November and high speed records showed that the signals, when present, consisted of a series of pulses each lasting $\sim 0·3$ s and with a repetition period of about 1·337 s which was soon found to be maintained with extreme accuracy. Further observations have shown that the true period is constant to better than 1 part in 10^7 although there is a systematic variation which can be ascribed to the orbital motion of the Earth. The impulsive nature of the recorded signals is caused by the periodic passage of a signal of descending frequency through the 1 MHz pass band of the receiver.

of three others having remarkably similar properties which suggests that this type of source may be relatively common at a low flux density. A tentative explanation of these unusual sources in terms of the stable oscillations of white dwarf or neutron stars is proposed.

Position and Flux Density

The aerial consists of a rectangular array containing 2,048 full-wave dipoles arranged in sixteen rows of 128 elements. Each row is 470 m long in an E.–W. direction and the N.–S. extent of the array is 45 m. Phase-scanning is employed to direct the reception pattern in declination and four receivers are used so that four different declinations may be observed simultaneously. Phase-switching receivers are employed and the two halves of the aerial are combined as an E.–W. interferometer. Each row of dipole elements is backed by a tilted reflecting screen so that maximum sensitivity is obtained at a declination of approximately $+30°$, the overall sensitivity being reduced by more than one-half when the beam is scanned to declinations above $+90°$ and below $-5°$. The beamwidth of the array to half intensity is about $\pm \frac{1}{2}°$ in right ascension and $\pm 3°$ in declination; the phasing arrangement is designed to produce beams at roughly $3°$ intervals in declination. The receivers have a bandwidth of 1 MHz centred at a frequency of 81·5 MHz and routine recordings are made with a time constant of 0·1 s; the r.m.s. noise

Instantaneous Bandwidth and Frequency Drift

Two different experiments have shown that the pulses are caused by a narrow-band signal of descending frequency sweeping through the 1 MHz band of the receiver. In the first, two identical receivers were used, tuned to frequencies of 80·5 MHz and 81·5 MHz. Fig. 1d, which

Pulse Recurrence Frequency and Doppler Shift

By displaying the pulses and time pips from *MSF* Rugby on the same record the leading edge of a pulse of reasonable size may be timed to an accuracy of about 0·1 s. Observations over a period of 6 h taken with the tracking system mentioned earlier gave the period between pulses as $P_{obs} = 1·33733 \pm 0·00001$ s. This represents a mean value centred on December 18, 1967, at 14 h 18 m UT. A study of the systematic shift in the frequency of

This yields $\varphi = 43° \ 36' \pm 30'$ which corresponds to a declination of $21° \ 58' \pm 30'$, a value consistent with the declination obtained directly. The true periodicity of the source, making allowance for the Doppler shift and using the integral condition to refine the calculation, is then

$$P_0 = 1·3372795 \pm 0·0000020 \ s$$

The Nature of the Radio Source

The lack of any parallax greater than about 2' places the source at a distance exceeding 10^3 A.U. The energy emitted by the source during a single pulse, integrated over 1 MHz at 81·5 MHz, therefore reaches a value which must exceed 10^{17} erg if the source radiates isotropically.
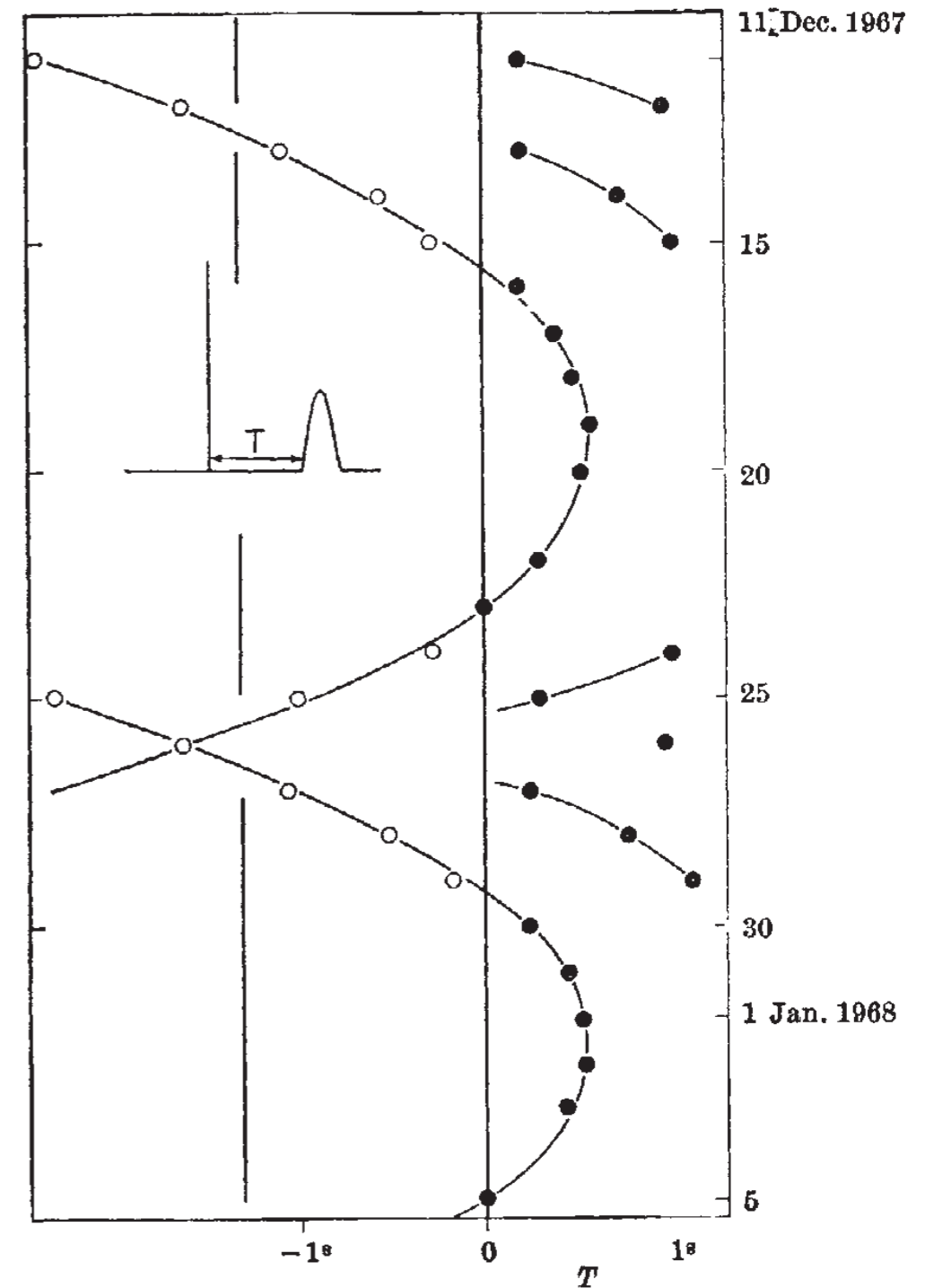
Pulsar discovery : Nature 1968
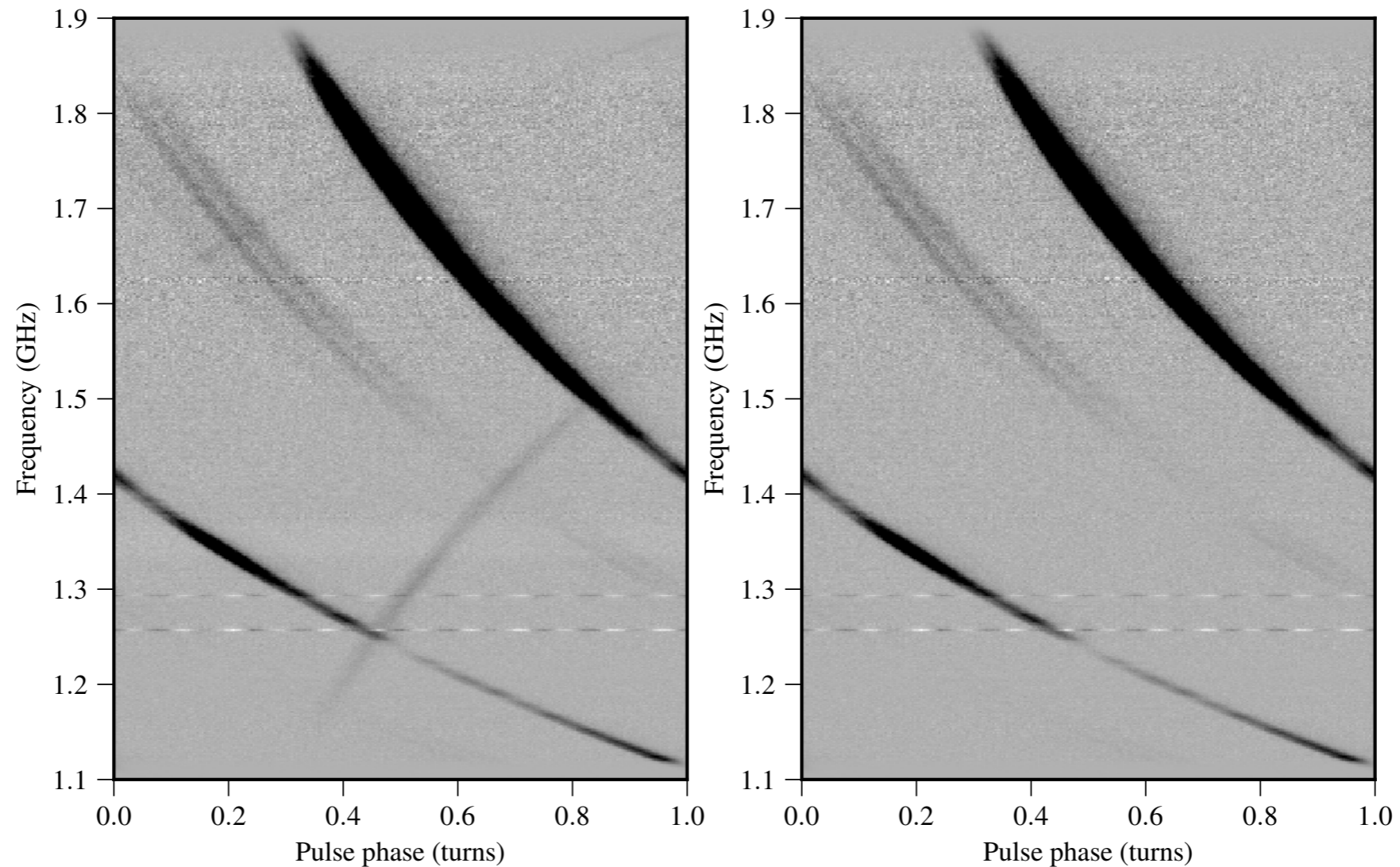

Fig. 4. The day to day variation of pulse arrival time.
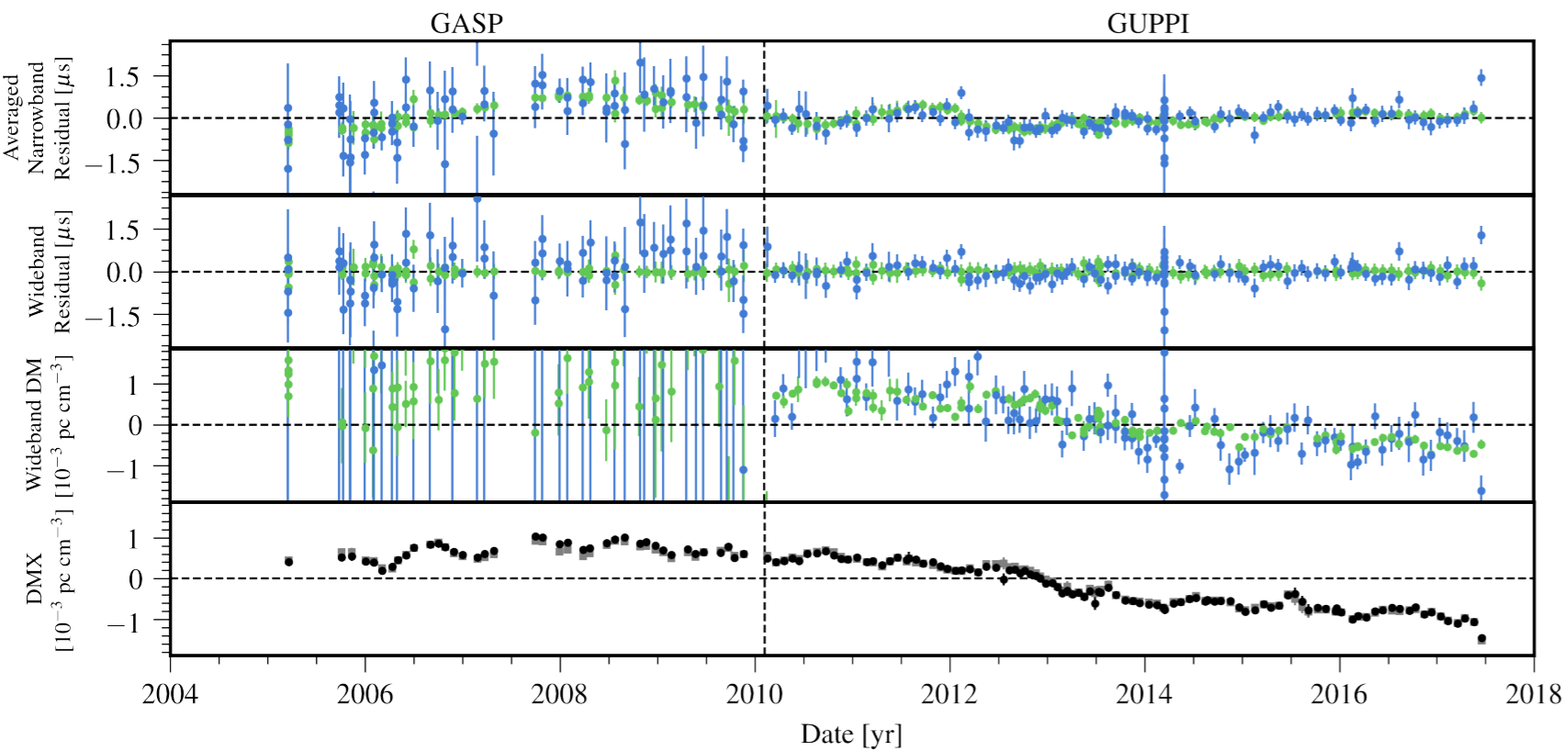
DM : dispersion measure …

Web page on Dispersion Measure
(astronomy@swinburn)

DM : dispersion due to propagation in the ionised interstellar medium

Figure 2. Observation of J1744+1134 illustrating artifacts from GUPPI's interleaved ADCs. This is one of the lowest-DM pulsars in our sample, therefore the effect is easily visible. Dispersion has not been removed, so the true pulsar signal arrives earlier at higher radio frequencies. The image artifact can be seen as the faint, apparently negatively-dispersed, signal "reflected" about the band center frequency of 1.5 GHz. No interference excision has been applied to these data; the spurious narrowband signals visible between 1.2 and 1.3 GHz are RFI. The plot color scale has been saturated at 10% of the maximum data value. The left panel shows the raw data, while the right panel shows the same data after the correction procedure has been applied.
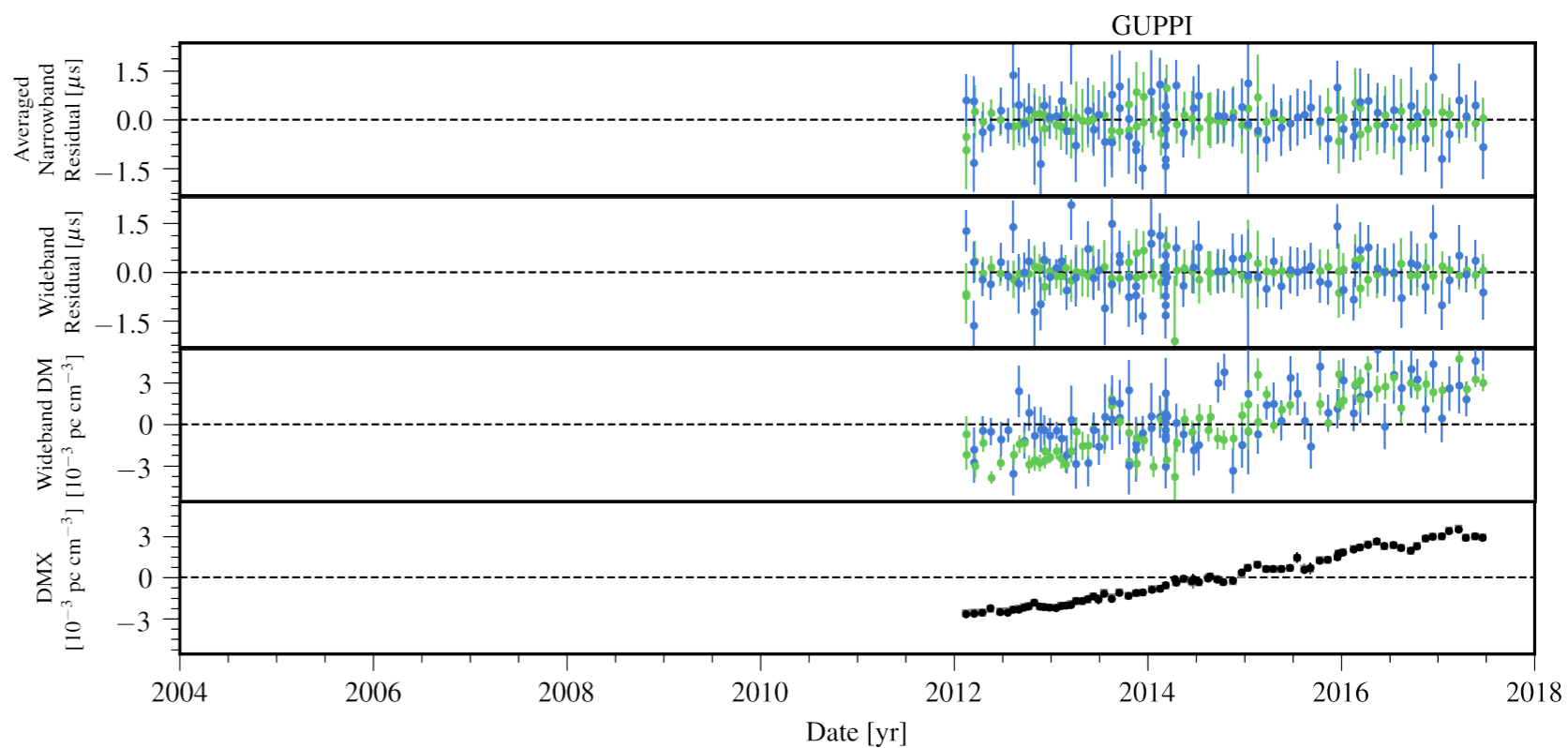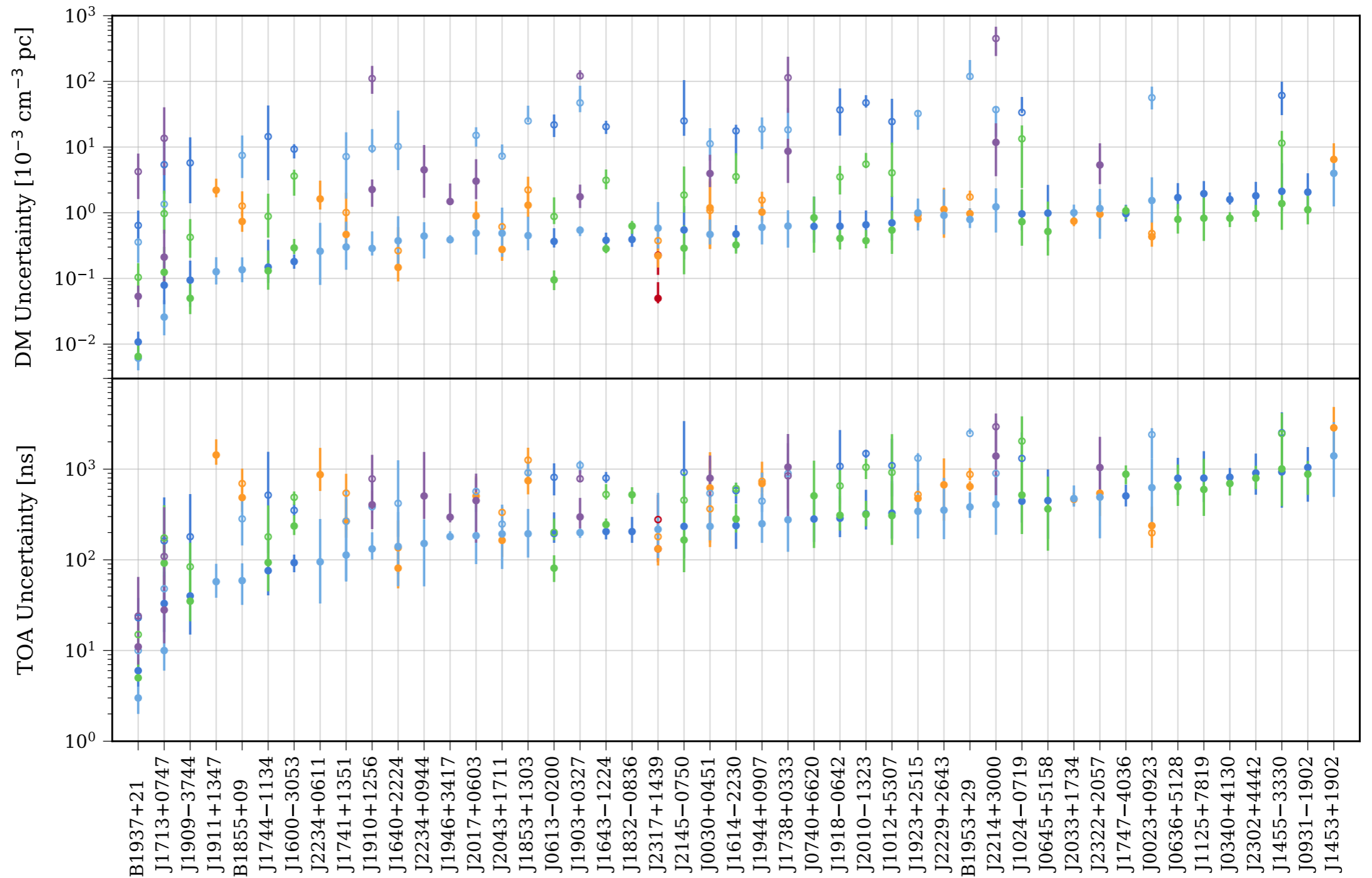
J0613−0200

Dispersion : frequency dependent
propagation velocity due to ionised
interstellar medium - mostly
determined by the integrated
electron density along the line of
sight:

$$\frac{d\nu}{dt} = -\frac{c}{L}\frac{\nu^3}{\nu_p^2}$$

$$\nu_p = \frac{1}{2\pi}\sqrt{\frac{n_e e^2}{m_e^* \epsilon_0}}$$
(Plasma frequency)

J0340+4130

Figure 2. The median raw wideband TOA and DM measurement uncertainties with central 68% intervals. Pulsars are ordered by their median PUPPI or GUPPI L-band (1.4 GHz) TOA uncertainties. The dramatic increase in DM precision after moving from the ASP and GASP backends (open cirlces) to the PUPPI and GUPPI backends (filled circles) is evident. The colors indicate the receiver as in Figure 1: 327 MHz (red), 430 MHz (orange), 820 MHz (green), 1.4 GHz (lighter blue for AO, darker blue for the GBT), 2.1 GHz (purple).

https://arxiv.org/abs/2005.06495
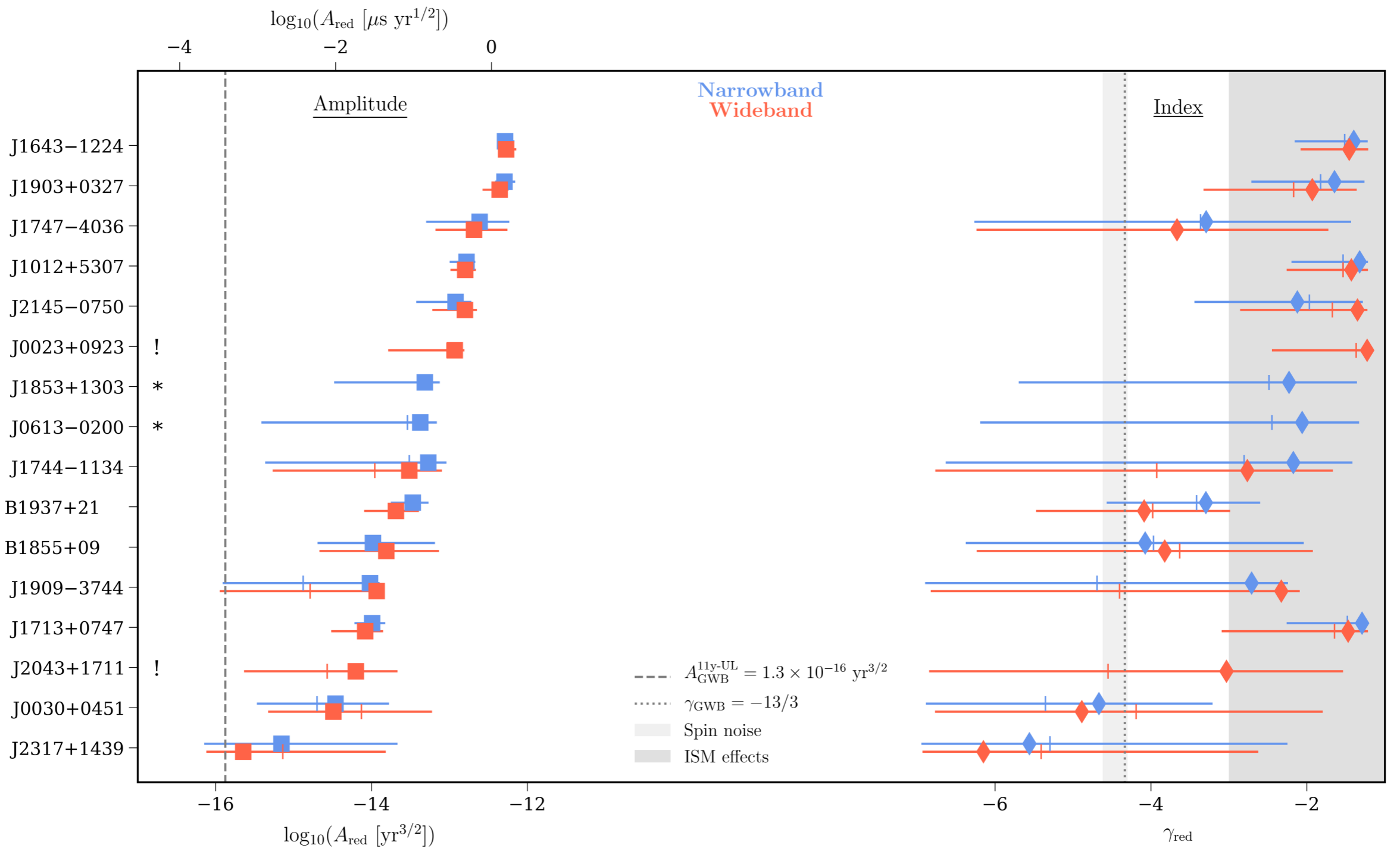
Figure 7. Comparison of the significantly detected power-law red noise parameters in the two data sets; measurements from the wideband data set are plotted below those from NG12.5. Pulsars are ordered top-to-bottom by highest-to-lowest red noise amplitude seen in the wideband data set, and the large symbols represent the MAP parameter estimates: squares indicate the logarithm of the amplitude at a frequency of $1\,\mathrm{yr}^{-1}$ (dual units shown), and diamonds represent the power-law index. The central 95% of the marginalized posterior distribution for each parameter is shown as a line with a tick indicating the median. Two pulsars have above-threshold red noise seen in the narrowband data set, but not in the wideband data set (indicated with ∗), and two pulsars have the reverse situation (indicated with !). The apparent correlation between red noise amplitude and

From timing residuals to GWB signal strength

https://arxiv.org/abs/2009.04496

From timing residuals to GW strength

- ✤ Analysis of timing residual δt = f(time) data sets to search for time correlated signals, auto and cross correlations between pulsars

- ✤ Comparison with models including various sources of time correlated signals, modelled mostly as power law (or broken power law) in frequency

3.1. *Models of time-correlated processes*

The principal results of this paper are referred to a fiducial power-law spectrum of characteristic GW strain

$$h_c(f) = A_{\mathrm{GWB}} \left(\frac{f}{f_{\mathrm{yr}}} \right)^{\alpha}, \qquad (1)$$

with $\alpha = -2/3$ for a population of inspiraling SMBHBs in circular orbits whose evolution is dominated by GW emission (Phinney 2001). We performed our analysis in terms of the timing-residual cross-power spectral density

$$S_{ab}(f) = \Gamma_{ab} \frac{A_{\mathrm{GWB}}^2}{12\pi^2} \left(\frac{f}{f_{\mathrm{yr}}} \right)^{-\gamma} f_{\mathrm{yr}}^{-3}. \qquad (2)$$

where $\gamma = 3 - 2\alpha$ (so the fiducial SMBHB $\alpha = -2/3$ corresponds to $\gamma = 13/3$), and where Γ_{ab} is the overlap reduction function (ORF), which describes average correlations between pulsars a and b in the array as a function of the angle between them. For an isotropic GWB, the ORF is given by Hellings & Downs (1983) and we refer to it casually as "quadrupolar" or "HD" correlations.

3.5. *Optimal Statistic*

As in NG9b, we perform a frequentist GWB analysis using the optimal statistic $\hat{A}_{\mathrm{GWB}}^2$, a point estimator for the amplitude of an isotropic GW stochastic background (Anholm et al. 2009; Chamberlin et al. 2015). This statistic accounts implicitly for interpulsar spatial correlations. The estimator is derived by maximizing the PTA likelihood analytically, and it can be written as

$$\hat{A}_{\mathrm{GWB}}^2 = \frac{\sum_{ab} \delta t_a^T P_a^{-1} \tilde{S}_{ab} P_b^{-1} \delta t_b}{\sum_{ab} \mathrm{Tr}\,(P_a^{-1} \tilde{S}_{ab} P_b^{-1} \tilde{S}_{ba})}, \qquad (7)$$

where δt_a is the vector of timing residuals for pulsar a, $P_a = \langle \delta t_a \delta t_a^T \rangle$ is the autocovariance matrix of the residuals, and $\hat{A}_{\mathrm{gw}}^2 \tilde{S}_{ab} = S_{ab} = \langle \delta t_a \delta t_b^T \rangle|_{a \neq b}$ is the cross-covariance matrix between the residuals for pulsars a and b. The average signal-to-noise ratio (S/N) of the optimal statistic is

$$\langle \rho \rangle = A_{\mathrm{gw}}^2 \left[\sum_{ab} \mathrm{Tr}\,(P_a^{-1} \tilde{S}_{ab} P_b^{-1} \tilde{S}_{ba}) \right]^{1/2}, \qquad (8)$$

https://arxiv.org/abs/2009.04496

https://arxiv.org/abs/1801.02617 (NG11gwb)

Table 1. Data models.

| NG11gwb labels	1	2A	2B	2D	3A	(new)	3B	3D
spatial correlations		single common- spectrum process				two common- spectrum processes		
• uncorrelated		✓				✓		
• dipole			✓				✓	
• monopole				✓				✓
• HD					✓	✓	✓	✓
pulsar-intrinsic red-noise	✓	✓	✓	✓	✓	✓	✓	✓

NOTE—The data models analyzed in this paper are organized by the presence of spatially-correlated common-spectrum noise processes. Model names are added for a direct comparison to the naming scheme employed in NG11gwb.
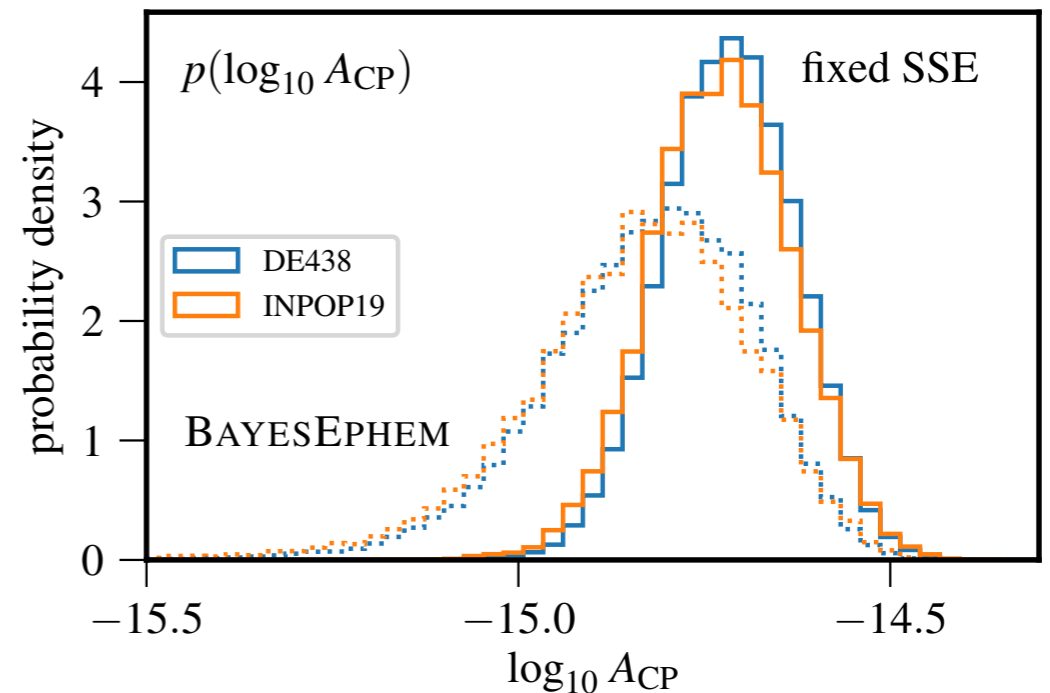
Figure 2. Bayesian posteriors for the $(f_{yr} = 1yr^{-1})$ amplitude A_{CP} of a common-spectrum process, modeled as a $\gamma = 13/3$ power law using only the lowest five component frequencies. The posteriors are computed for the NANOGrav 12.5-year data set using individual ephemerides (solid lines), and BAYESEPHEM (dotted). Unlike similar analyses in NG11gwb and Vallisneri et al. (2020), these posteriors, even those using BAYESEPHEM imply a strong pref-

Detection of a common-spectrum process in NG12

Figure 1. Posteriors for a common-spectrum process in NG12, as recovered with four models: free-spectrum (gray violin plots in left panel), broken power law (solid blue lines and contours), five frequency power law (dashed orange lines and contours), and 30 frequency power law (dot-dashed green lines and contours). In the left panel, the violin plots show marginalized posteriors of
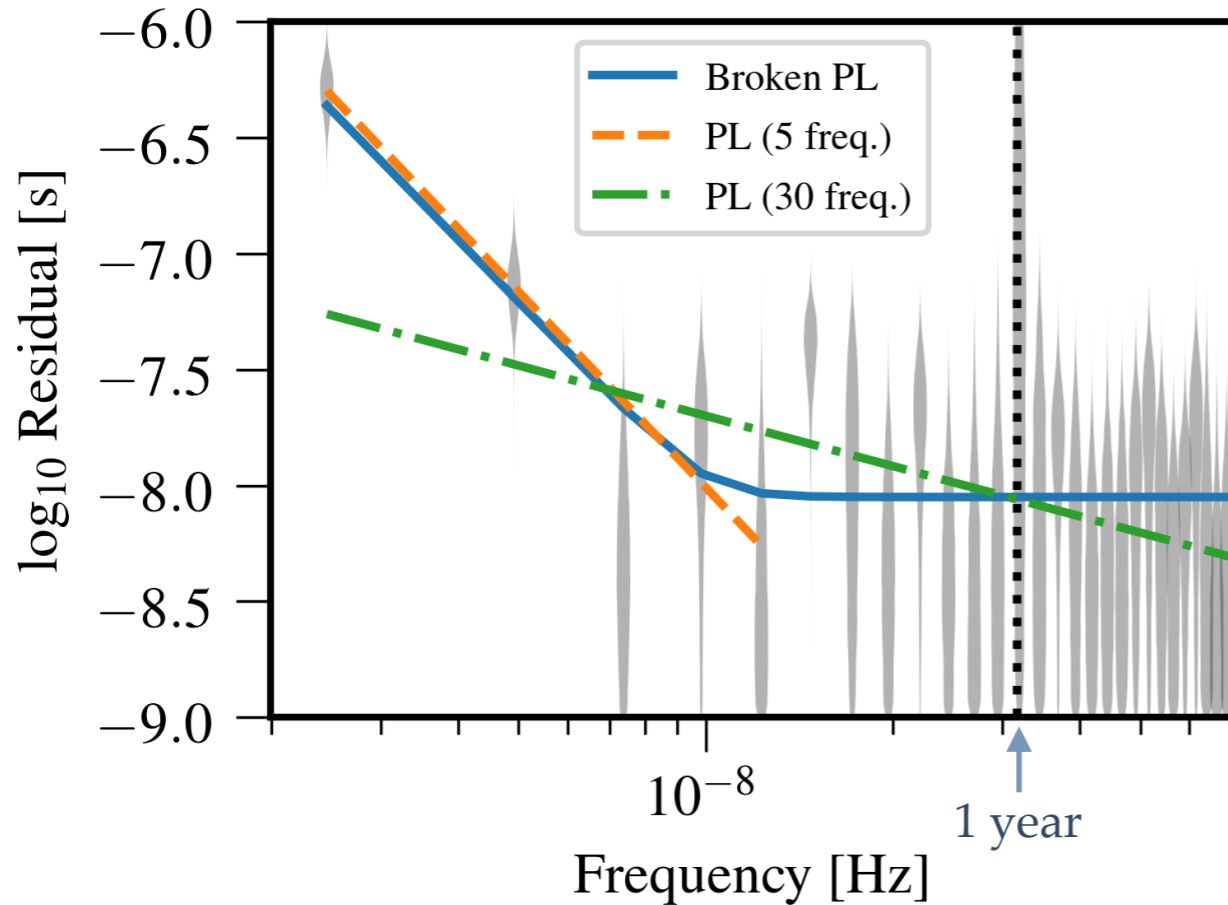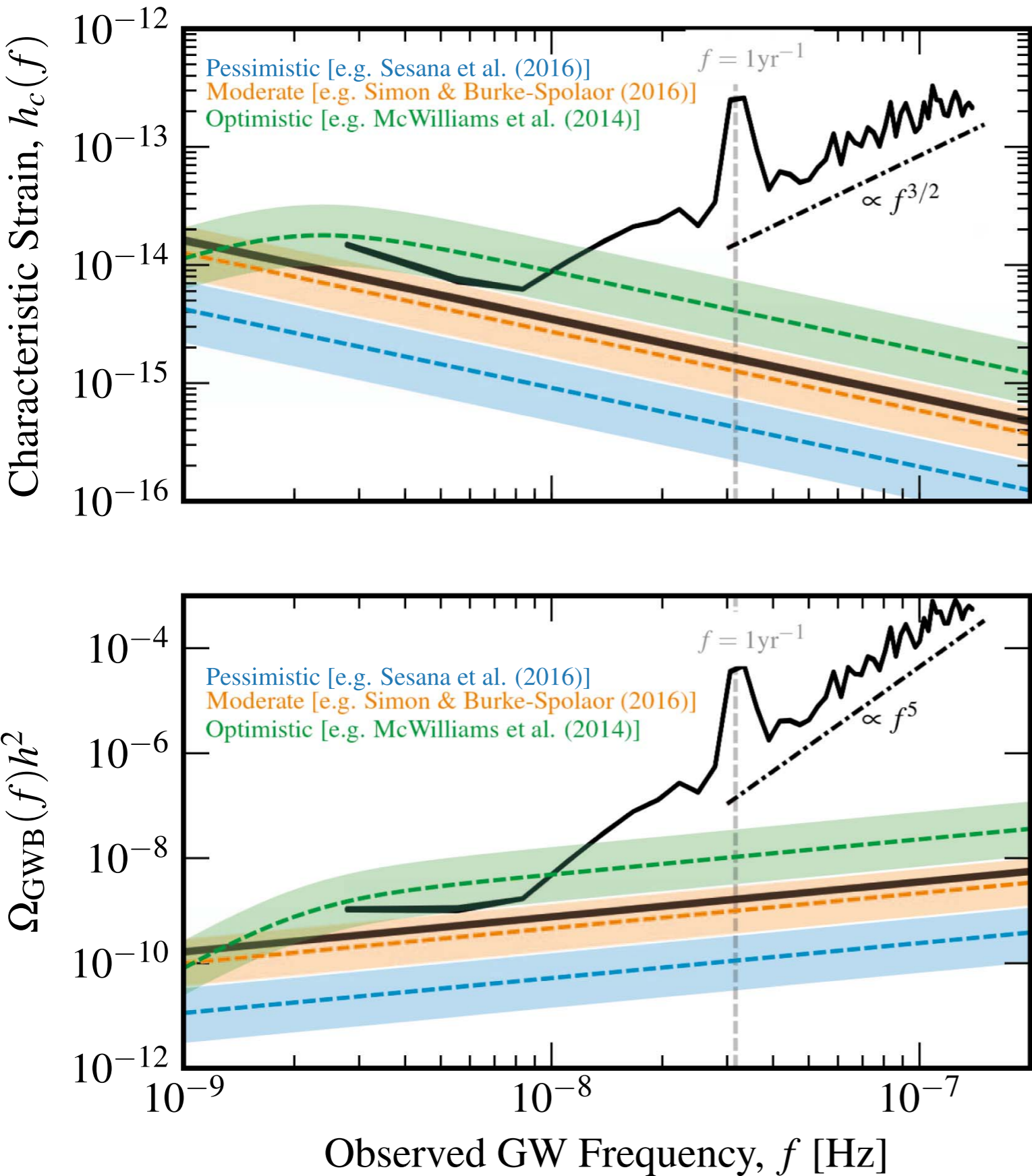

Timing residuals (TOA, Time of Arrival) as a function of frequency (excess red noise)
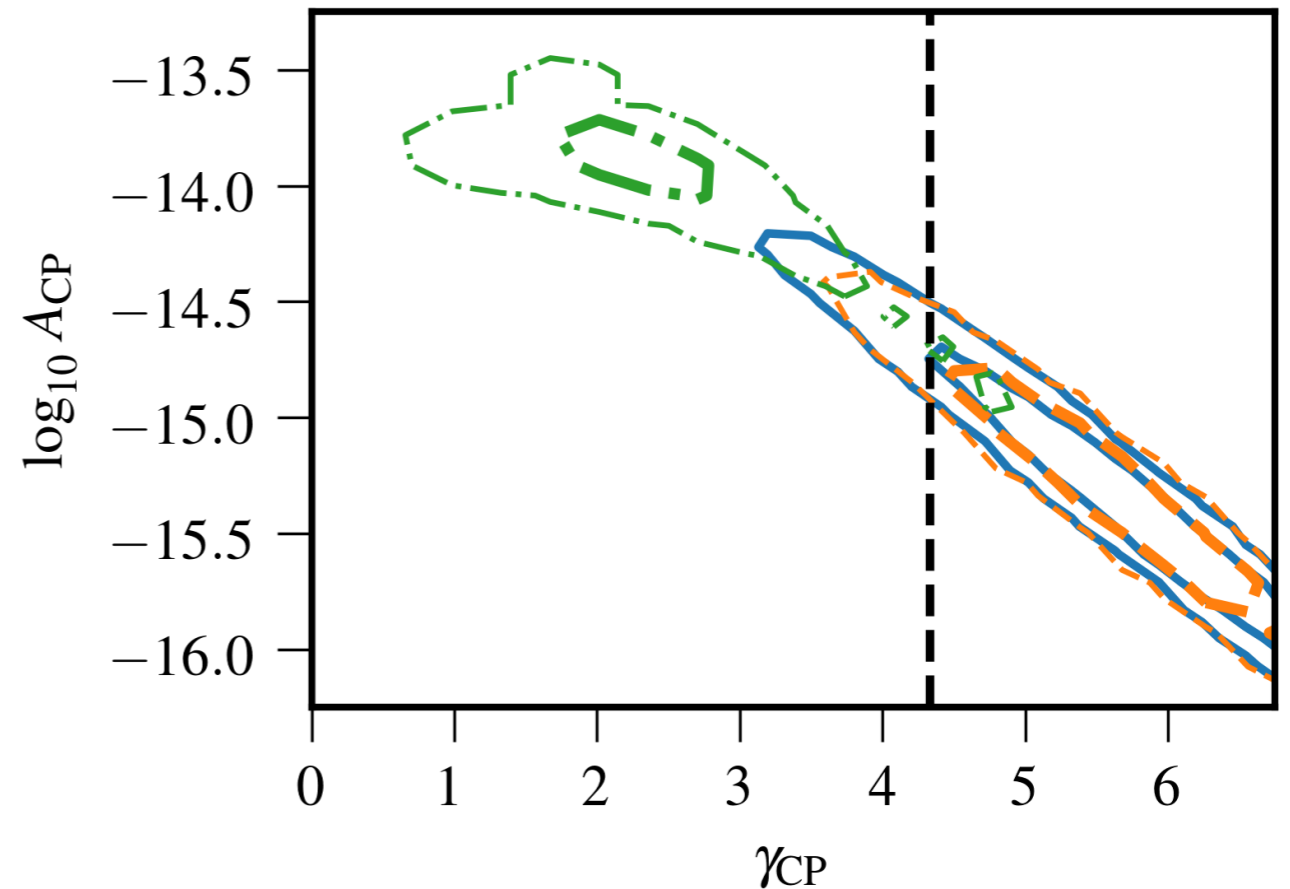
Fitted power law slope and amplitude - Broken power law model , 5, 30 component variable index

Broken power law model
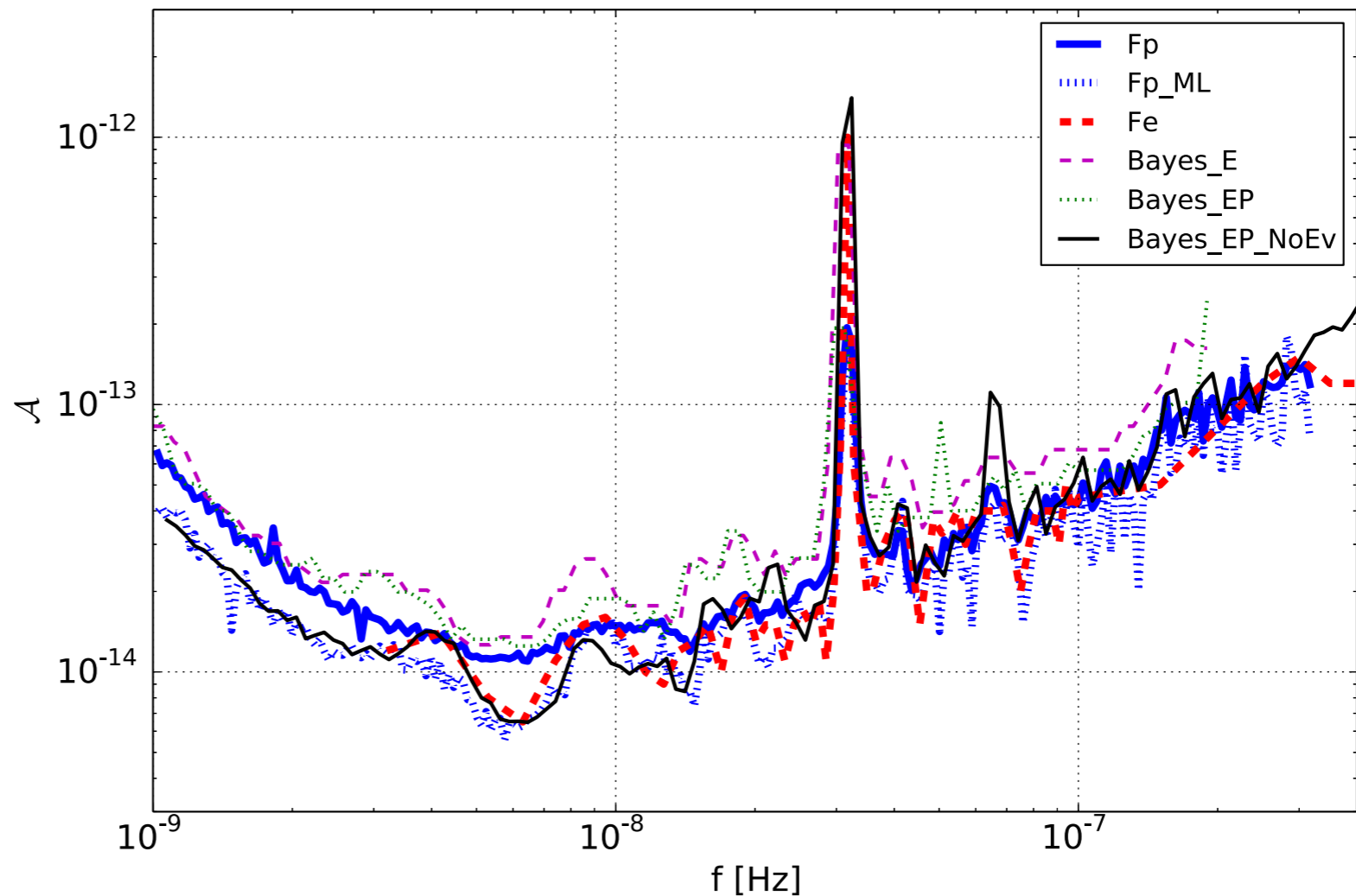
$$S(f) = \frac{A_{\text{GWB}}^2}{12\pi^2} \left(\frac{f}{f_{\text{yr}}}\right)^{-\gamma} \left(1 + \left(\frac{f}{f_{\text{bend}}}\right)^{1/\kappa}\right)^{\kappa(\gamma-\delta)} f_{\text{yr}}^{-3},$$

(3)

Figure 3. Top panel: GWB amplitude 95% upper limits for an uncorrelated common process with a $\gamma = 13/3$ power law (straight black line) or with independently determined free-spectrum components (jagged black line). The thickness of the lines spans the spread of results over different ephemerides. The dashed–dotted line shows the expected sensitivity scaling behavior for white noise. The colored dashed lines and bands show the median and one-sigma ranges for the GWB amplitudes predicted in MOP14 (green), Simon & Burke-Spolaor (2016; orange), and S16 (blue). Bottom panel: as in the top panel, except showing the results in terms of the stochastic GWB energy density (per logarithmic frequency bin) in the universe as a fraction of closure density, $\Omega_{\mathrm{GWB}}(f)h^2$. The relationship between $h_c(f)$ and $\Omega_{\mathrm{GWB}}(f)h^2$ is given in Equation (10).

https://arxiv.org/abs/1509.02165 (EPTA)

European Pulsar Timing Array limits on continuous gravitational waves
**from individual supermassive black hole binaries**

noise only. Depending on the adopted detection algorithm, the 95 per cent upper limit on the sky-averaged strain amplitude lies in the range $6 \times 10^{-15} < A < 1.5 \times 10^{-14}$ at $5\,\mathrm{nHz} < f < 7\,\mathrm{nHz}$. This limit varies by a factor of five, depending on the assumed source position and the most constraining limit is achieved towards the positions of the most sensitive pulsars in the timing array. The most robust upper limit – obtained via a full Bayesian analysis searching simultaneously over the signal and pulsar noise on the subset of ours six best pulsars – is $A \approx 10^{-14}$. These limits, the most stringent to date at $f < 10\,\mathrm{nHz}$, exclude the presence of sub-centiparsec binaries with chirp mass $\mathcal{M}_c > 10^9\,\mathrm{M}_\odot$ out to a distance of about 25 Mpc, and with $\mathcal{M}_c > 10^{10}\,\mathrm{M}_\odot$ out to a distance of about 1 Gpc ($z \approx 0.2$). We show that state-of-

Figure 6. The 95 per cent upper limit on the GW strain for the three frequentist methods, i.e. $\mathcal{F}_p$ varying noise (*Fp*), $\mathcal{F}_p$ fixed noise (*Fp_ML*) and $\mathcal{F}_e$, and the three bayesian methods, i.e. "evolving source" with Earth term only (*Bayes_E*) and with Earth and Pulsar terms (*Bayes_EP*) and 'non-evolving source with Earth and Pulsar terms (*Bayes_EP_NoEv*), see Table 1 for details.
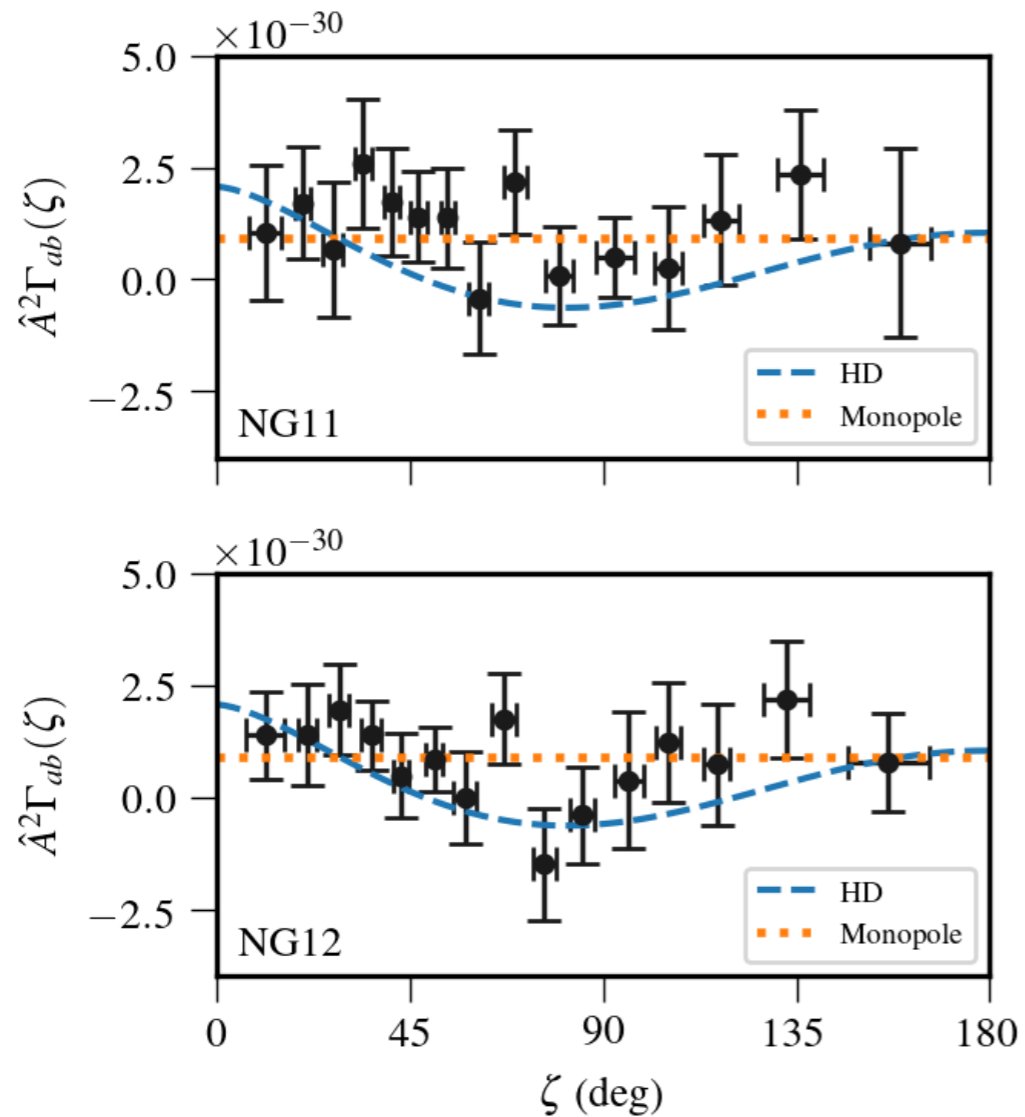
Figure 5. Average angular distribution of cross-correlated power, as estimated with the optimal statistic on the 11-year data set (*top*) and 12.5-year data set (*bottom*). The number of pulsar pairs in each binned point is held constant for each data set. Due to the increase in pulsars in the 12.5-yr data set, the number of pairs per bin increases accordingly. Pulsar-intrinsic red-noise amplitudes are set to their maximum posterior values from the Bayesian analysis, while the
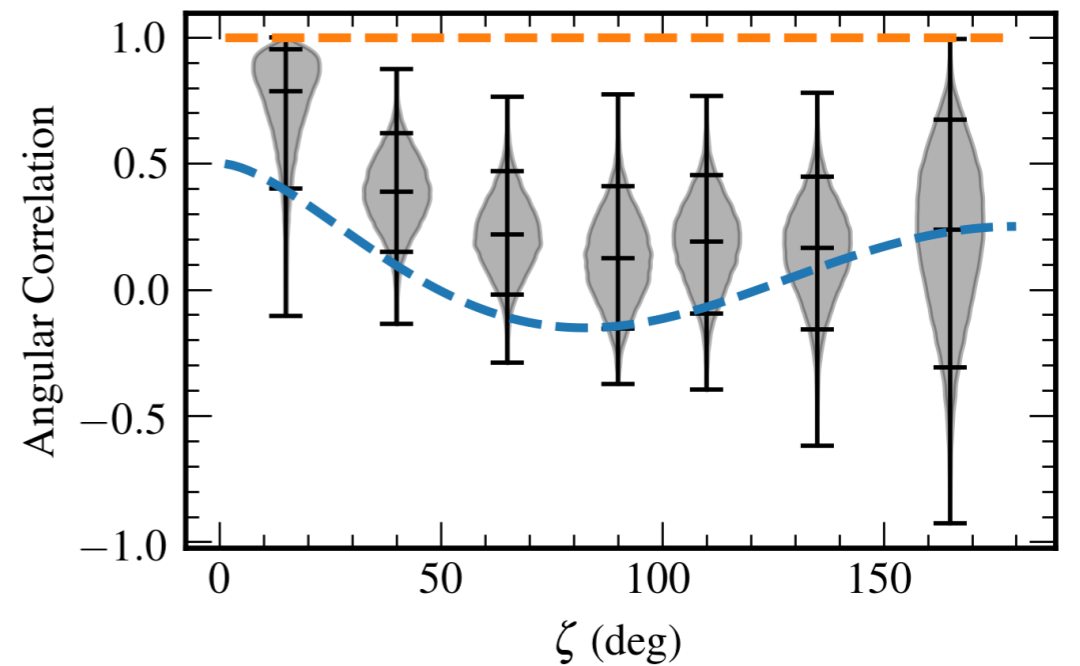
Figure 7. Bayesian reconstruction of inter-pulsar spatial correlations, parametrized as a seven-node spline. Violin plots show marginalized posteriors for node correlations, with medians, 5% and 95% percentiles, and extreme values. The dashed blue line shows the HD ORF expected for a GWB, while the dashed horizontal orange line shows the expected inter-pulsar correlation signature for a monopole systematic error, e.g. drifts in clock standards.

Conclusions ? let's look at the author's own conclusions ...

6.3. *Expectations for the Future*

The analysis of NANOGrav pulsar timing data presented in this paper is the first PTA search to show ==definite evidence for a common-spectrum stochastic signal across an array of pulsars.== ==However, evidence for the tell-tale quadrupolar HD-correlations is currently lacking, and there are other potential contributors to a common-spectrum process.== A majority of the pulsars with long observational baselines show the strongest evidence for a common-spectrum process; this subset of pulsars could be starting to show similar spin noise with a consistent spectral index. However, it is unlikely that strong spin noise would appear at a similar amplitude in all millisecond pulsars (Lam et al. 2017). Additionally, the per-pulsar evidence is significantly reduced

when we apply BAYESEPHEM, as expected; there remain other solar system effects for which we do not directly account, such as planetary Shapiro delay (Hobbs & Edwards 2012), that could contribute to the common-spectrum process. Finally, there are other sources of systematic noise that we may have uncovered (Tiburzi et al. 2016), and the further potential for sources yet to be diagnosed, all of which would require further study to isolate. ==Thus, attributing the signal uncovered in this work to an astrophysical GWB will necessitate verification with independent pipelines on larger (and/or independent) data sets.==
One avenue to validate the processing of timing observations will be the analysis of the "wideband" version of

Thank you for your attention